Order Number 9108106

Relativistic quasiparticle description of the structure of finite nuclei

Gao, Shun-fu, Ph.D.

City University of New York, 1990

U·M·I
300 N. Zeeb Rd.
Ann Arbor, MI 48106

RELATIVISTIC QUASIPARTICLE DESCRIPTION OF THE STRUCTURE OF FINITE NUCLEI

by

SHUN-FU GAO

A dissertation submitted to the Graduate Faculty in Physics in partial fulfillment of the requirements for the degree of Doctor of Philosophy, The City University of New York

1990

This manuscript has been read and accepted for the Graduate Faculty in Physics in satisfaction of the dissertation requirement for the degree of Doctor of Philosophy.

7-10-90
Date

Chair of Examining Committee

7-24-90
Date

Executive Officer

C.M. Shakin

L.S. Celenza

V. Franco

P. Lesser

J. Birman

Supervisory Committee

The City University of New York

Abstract

RELATIVISTIC QUASIPARTICLE DESCRIPTION OF

THE STRUCTURE OF FINITE NUCLEI

by

Shun-fu Gao

Adviser: Distinguished Professor Carl M. Shakin

In an attempt to understand the success of Dirac phenomenology, Professors Celenza and Shakin proposed the so-called Relativistic-Brueckner-Hartree-Fock (RBHF) theory (Ref.5) which is characterized as having no free parameters other than those introduced in fitting free-space nucleon-nucleon scattering data.

A natural extension of the relativistic analysis of Ref.5 lies in the study of the structure of finite nuclei. To avoid the formidable task of calculating relativistic Brueckner reaction matrices for a finite system, we use an effective interaction constructed for use in a Dirac-Hartree-Fock Calculation. This interaction reproduces, rather accurately, the nucleon self-energy in nuclear matter, the Migdal

parameters and the saturation curves obtained via RBHF calculations.

We used this effective interaction in Dirac-Hartree-Fock calculations of the structure of the finite nuclei, ^{16}O and ^{40}Ca. We performed these calculations in momentum space and maintained translational invariance in our analysis. We have calculated the binding energies, nucleon energy levels, wave functions and the charge distributions for ^{16}O and ^{40}Ca. We find a good representation of the charge density of these nuclei and some degree of underbinding, which, in part, reflects the underbinding of nuclear matter for the one-boson-exchange potential (OBEP) whose reaction matrices are simulated by our effective interaction.

Acknowledgements

To Professor Carl M. Shakin, my thesis advisor, I wish to express my deepest gratitude for his valuable guidance and constant encouragement throughout this thesis work.

I would also like to express my sincere gratitude to Professor Louis S. Celenza of Brooklyn College of CUNY for the help given to me during the course of this work.

I would like to express my special thanks to Professor and Mrs. Shakin for providing "Math-Text" software for my use.

I wish to acknowledge, with gratitude, the Department of Physics of Brooklyn College, the Research Foundation of CUNY and the Graduate School of CUNY for financial support during the course of this work. I also wish to express my gratitude to the Brooklyn College Computer Center, the CUNY Computer Center and the Cornell National super-computer Center for allowing me the use of their facilities.

CONTENTS

List of Tables

List of Figures

Chapter 1

General Survey

1.1 Introduction

One of the principal goals of theoretical nuclear physics is to understand nuclear structure in terms of the free nucleon-nucleon interaction. In the past, our ideas concerning nuclear structure were essentially based upon an analogy with atomic physics. One considered the nucleus to be a collection of nucleons which interacted through two-body potentials. Such models had their limitations, since one did not explain the origin of the potentials. After 1935, in an attempt to understand the nature of nucleon interactions, one saw the formulation of meson theory. Meson theory is formulated as a quantum field theory. Such a formulation is especially suitable for perturbative methods. However, since perturbative methods are not particularly successful in strong interaction physics, researchers have used effective interactions and phenomenological approaches in the context of Schroedinger theory.

The program of calculating the properties of nuclei and nuclear matter from "realistic" two-body forces was initiated by Brueckner and his collaborators about 1955. The reaction matrix formalism of nuclear many-body theory (Brueckner theory) has been widely used since 1958. The Brueckner G-matrix describes the interaction of two nucleons in the nuclear medium and is the analogue of the scattering matrix for two nucleons in free space. One of the main obstacles to a direct application of the Hartree-Fock method is the fact that most bare nucleon-nucleon forces have an infinite or strongly repulsive core. The replacement of the bare interaction by the Brueckner G-matrix is convenient because it allows one to treat strongly repulsive forces and it can also be shown that the use of the G-matrix represents a consistent resummation of certain higher-order terms of the full many-body problem. The Brueckner theory achieved some qualitative success in explaining the ground-state properties of nuclear matter and closed-shell nuclei. After extensive efforts by many investigators, it was clear that there was a fundamental problem in obtaining a good fit to nuclear properties in a parameter-free model.

In the early seventies we saw the introduction of what was called "density-dependent-Hartree-Fock" (DDHF) theory. In the latter analysis

one introduced a phenomenological density dependence into the two-body interaction in the medium. This interaction could then be adjusted to obtain a reasonable fit to nuclear charge and matter distributions, binding energies, etc. However, the introduction of density-dependent forces and various parameters took one away from the goal of calculating nuclear properties in a parameter-free theoretical scheme.

In the early seventies we also saw extensive development of the boson-exchange model of nuclear forces. In this model the nucleon-nucleon force was constructed via the exchange of mesonic fields with the quantum numbers of familiar mesons: π, ρ, ω and σ, etc. When one used the OBE potentials to calculate the properties of nuclear matter, one found the standard problem: If the binding energy of the system was correct, the saturation density was too large, and if the density was correct, the system was underbound.

In the mid-seventies some new ideas were introduced which would ultimately change our view of nuclear structure. People started to use the Dirac equation with some effective potentials to solve some long standing puzzles in the theory of nuclear structure. B. C. Clark and collaborators showed that nucleon-nucleus scattering could best be

described by using a phenomenology based upon the use of the Dirac equation in the description of the motion of the projectile.

In an attempt to understand the phenomenological success of these models, Professors Celenza and Shakin proposed the so-called Relativistic-Brueckner-Hartree-Fock (RBHF) theory (Ref.5), which is characterized as having no free parameters other than those introduced in fitting free-space nucleon-nucleon scattering data. This theory was modeled after the Brueckner approach. However, the Brueckner analysis was extended to include a relativistic description of nucleon motion. While not providing a complete theory, the RBHF analysis does provide quite successful parameter-free model and leads to a deeper understanding of Dirac phenomenology. One was able to discuss such matters as the binding energy and saturation density of the nuclear matter, the effective force in nuclei, and the forms of the nucleon self-energy for bound and continuum nucleons.

One reason for the study of nuclear matter is that it provides a check on the suitability of a nucleon-nucleon potential before one starts doing extensive and complicated calculations in finite nuclei. (A numerical evaluation of nuclear matter properties is much easier,

since the wave functions of this system are known to be plane waves, while the wave functions of finite nuclei have to be determined self-consistently.) The necessity for a study of nuclear matter stems from the fact that the empirical nucleon-nucleon data do not sufficiently determine the form of the potential. Thus, a calculation of the properties of nuclear matter could rule out some unsuitable potential models.

A natural extention of the relativistic analysis in Ref.5 lies in the study of the structure of finite nuclei. (To that end one might contemplate the calculation of relativistic Brueckner reaction matrices for a finite system; however, that is an extremely difficult program, which we will not consider.) We note that one often wishes to obtain an effective interaction which may be used in the study of finite nuclei. Historically, in order to account for nuclear saturation, effective interactions are usually taken to be either density- or momentum-dependent, or both. Early attempts, which reproduced the nuclear properties at saturation density only, rarely included a study of other properties of nuclear matter, for instance, the effective interaction between nuclear quasi-particles. We are interested in an effective interaction which may be used in a Dirac-

Hartree-Fock approximation for the study of finite nuclei. This effective interaction should be "realistic" in the sense that matrix elements of the effective interaction should reproduce the nucleon self-energy, the saturation curves and the Migdal parameters calculated in Relativistic-Brueckner-Hartree-Fock studies of nuclear matter.

In this work we will study the properties of finite nuclei using the effective interaction we have obtained previously.

In Chapter 2 we review the model for the effective interaction. In Chapter 3 we derive the integral equations for the nucleon wave functions. In Chapter 4 we give some formulae related to the properties of finite nuclei. In Chapter 5 we present numerical results and some discussion. Chapter 6 contains some concluding remarks.

1.2 Notation and Conventions

We use the notation presented in the texts of Bjorken and Drell (Ref.14):

$$x^{\mu} = (x^0, \vec{x}) , \tag{1.2.1}$$

$$x_{\mu} = g_{\mu\nu} x^{\nu} = (x^0, -\vec{x}) , \tag{1.2.2}$$

where the metric tensor is

$$g^{\mu\nu} = g_{\mu\nu} = \begin{pmatrix} 1 & 0 & 0 & 0 \\ 0 & -1 & 0 & 0 \\ 0 & 0 & -1 & 0 \\ 0 & 0 & 0 & -1 \end{pmatrix} , \tag{1.2.3}$$

For any two four-vectors, p and q, we denote the scalar product by

$$p \cdot q = p_{\mu} q^{\mu} = p^0 q^0 - \vec{p} \cdot \vec{q} , \tag{1.2.4}$$

$$p^2 = p^{02} - \vec{p}^2 . \tag{1.2.5}$$

The Dirac spinors are defined as

$$u(\vec{p}, s) = \left[\frac{E(\vec{p})+m}{2m} \right]^{1/2} \begin{pmatrix} \chi_s \\ \dfrac{\vec{\sigma} \cdot \vec{p}}{E(\vec{p})+m} \chi_s \end{pmatrix} , \tag{1.2.6}$$

and

$$v(\vec{p},s) = \left[\frac{E(\vec{p})+m}{2m}\right]^{1/2} \begin{pmatrix} \dfrac{\vec{\sigma}\cdot\vec{p}}{E(\vec{p})+m}\,\chi_{-s} \\ \chi_{-s} \end{pmatrix} . \qquad (1.2.7)$$

They satisfy the Dirac equations

$$[\ \gamma^0 E(\vec{p}) - \vec{\gamma}\cdot\vec{p} - m\ ]\ u(\vec{p},s) = 0\ , \qquad (1.2.8)$$

$$[\ \gamma^0 E(\vec{p}) - \vec{\gamma}\cdot\vec{p} + m\ ]\ v(\vec{p},s) = 0\ . \qquad (1.2.9)$$

The adjoint spinors

$$\bar{u}(\vec{p},s) = u^+(\vec{p},s)\gamma^0\ , \qquad (1.2.10)$$

$$\bar{v}(\vec{p},s) = v^+(\vec{p},s)\gamma^0\ , \qquad (1.2.11)$$

satisfy

$$\bar{u}(\vec{p},s)\ (\not{p} - m\ ) = 0\ , \qquad (1.2.12)$$

$$\bar{v}(\vec{p},s)\ (\not{p} + m\ ) = 0\ , \qquad (1.2.13)$$

where

$$\not{p} = \gamma^{\mu} p_{\mu} = \gamma^0 p^0 - \vec{\gamma} \cdot \vec{p} \ , \tag{1.2.14}$$

$$\gamma^0 = \begin{pmatrix} \mathbb{I} & 0 \\ 0 & -\mathbb{I} \end{pmatrix} , \tag{1.2.15}$$

and

$$\vec{\gamma} = \begin{pmatrix} 0 & \vec{\sigma} \\ -\vec{\sigma} & 0 \end{pmatrix} . \tag{1.2.16}$$

Here $\mathbb{I}$ is a 2x2 unit matrix and the σ are 2x2 Pauli spin matrices

$$\vec{\sigma} = (\sigma^1, \sigma^2, \sigma^3) , \tag{1.2.17}$$

$$\sigma^1 = \begin{pmatrix} 0 & 1 \\ 1 & 0 \end{pmatrix} , \quad \sigma^2 = \begin{pmatrix} 0 & -i \\ i & 0 \end{pmatrix} , \quad \sigma^3 = \begin{pmatrix} 1 & 0 \\ 0 & -1 \end{pmatrix} . \tag{1.2.18}$$

Frequently used combinations are

$$\sigma^{\mu\nu} = \frac{i}{2} \left[\gamma^{\mu}, \gamma^{\nu} \right] , \tag{1.2.19}$$

and

$$\gamma^5 = i\gamma^0\gamma^1\gamma^2\gamma^3 = \gamma_5 \ . \qquad (1.2.20)$$

In the above representation

$$\sigma^{ij} = \begin{pmatrix} \sigma^k & 0 \\ 0 & \sigma^k \end{pmatrix} , \qquad (1.2.21)$$

with i,j,k in cyclic order and

$$\sigma^{0i} = i \begin{pmatrix} 0 & \sigma^i \\ \sigma^i & 0 \end{pmatrix} , \qquad (1.2.22)$$

$$\gamma^5 = \gamma_5 = \begin{pmatrix} 0 & \mathbb{I} \\ \mathbb{I} & 0 \end{pmatrix} . \qquad (1.2.23)$$

The following identities and trace theorems have been used in our calculations.

$$\not{A}\not{B} = 2\ A\cdot B - \not{B}\not{A} , \qquad (1.2.24)$$

$$\gamma^\mu \not{A} \gamma_\mu = -\ 2\ \not{A} , \qquad (1.2.25)$$

$$\gamma^\mu \not{A}\not{B} \gamma_\mu = 4\ A\cdot B , \qquad (1.2.26)$$

$$\gamma^\mu \not{A} \not{B} \not{C} \gamma_\mu = - 2 \not{C} \not{B} \not{A} \ , \tag{1.2.27}$$

$$\mathrm{Tr}\ \mathbb{1} = 4 \ , \tag{1.2.28}$$

$$\mathrm{Tr}\ (\ \text{odd number of}\ \gamma^\mu\ ) = 0 \ , \tag{1.2.29}$$

$$\mathrm{Tr}\ \gamma^5 = 0 \ , \tag{1.2.30}$$

$$\mathrm{Tr}\ \not{A} \not{B} = 4\ A{\bullet}B \ , \tag{1.2.31}$$

$$\mathrm{Tr}\ \gamma^5 \not{A} \not{B} = 0 \ , \tag{1.2.32}$$

$$\mathrm{Tr}\ \not{A} \not{B} \not{C} \not{D} = 4\ [\ A{\bullet}B\ C{\bullet}D - A{\bullet}C\ B{\bullet}D + A{\bullet}D\ B{\bullet}C\ ] \ , \tag{1.2.33}$$

$$\mathrm{Tr}\ \gamma^5 \not{A} \not{B} \not{C} \not{D} = 4\ i\ \epsilon_{\alpha\beta\gamma\delta}\ A^\alpha\ B^\beta\ C^\gamma\ D^\delta \ . \tag{1.2.34}$$

1.3 Relativistic One-Boson-Exchange-Potentials

The formulation of the meson theory of nuclear forces took place more than 50 years ago. This model developed into the One-Boson-

Exchange potential model in the 1960's. In meson theory, the potential can be derived from a quantum field theory which describes meson exchange. The potential between a pair of nucleons due to the exchange of a meson has a range of the order of the meson Compton wavelength, which is inversely proportional to the meson mass. Various potentials (attractive or repulsive), spin-orbit potentials, tensor potentials, etc., have been derived by considering the exchange of different kinds of meson fields.

The pion-exchange contribution has a large range because of the small pion mass (140 MeV) and is responsible for the long-range part of the NN force. The scalar particle (with a mass of about 500 Mev) which is regarded as a convenient parameterization of the effect of corrected two-pion exchange (in an S-state) provides the intermediate-range attraction of the force. The repulsive inner region of the NN potential is thought to arise mainly from the exchange of massive vector mesons. The repulsion can be understood from the analogy with the Coulomb interaction, which is repulsive between two particles of like charge. The (neutral) vector meson (ω) can be considered as a massive (vector) photon and, therefore exchange of this meson will provide repulsion between nucleon pairs. The strong short-range spin-

orbit force then emerges as the Thomas term associated with vector meson exchange.

The interaction between nucleons and each of the scalar, pseudoscalar and vector bosons can take several forms. Usually the following interaction Lagrangians are considered

$$\mathcal{I}_s = g_s \bar{\psi} \psi \phi^{(s)} , \tag{1.3.1}$$

$$\mathcal{I}_{ps} = i g_{ps} \bar{\psi} \gamma^5 \psi \phi^{(ps)} , \tag{1.3.2}$$

$$\mathcal{I}_v = g_v \bar{\psi} \gamma^\mu \psi \phi_\mu^{(v)} + \frac{f_v}{4m} \bar{\psi} \sigma^{\mu\nu} \psi f_{\mu\nu}^{(v)} , \tag{1.3.3}$$

Here ψ denotes the nucleon field and $\bar{\psi}$ its adjoint; $\phi^{(\alpha)}$ describes the meson field of the α = scalar, pseudoscalar and vector mesons. For the exchange of isovector mesons (T = 1), $\phi^{(\alpha)}$ must be replaced by $\vec{\tau}\cdot\vec{\phi}$, where $\vec{\tau}$ is the isotopic spin operator. In Eq. (1.3.3)

$$f_{\mu\nu}^{(v)} = \partial_\mu \phi_\nu^{(v)} - \partial_\nu \phi_\mu^{(v)} , \tag{1.3.4}$$

represents the field strength; g_v and f_v describe the Dirac and Pauli

coupling constants, respectively. The corresponding terms give the Dirac and anomalous (Pauli) part of the magnetic moment.

For the pion (T = 1, $J^P = 0^-$), one has considered the pseudovector (pv) coupling, which reads as

$$\mathcal{L}_\pi = \frac{f_\pi}{m_\pi} \bar{\psi} \gamma^5 \gamma^\mu \vec{\tau} \cdot \frac{\partial \vec{\phi}(\pi)}{\partial x^\mu} \psi \ . \qquad (1.3.5)$$

We stress that, on the energy-shell, the pv- and ps- couplings lead to equivalent OPE potentials, provided we set

$$g_\pi^2 = \left[\frac{2m}{m_\pi} \right]^2 f_\pi^2 \ . \qquad (1.3.6)$$

Off energy-shell, however, these couplings behave quite differently. As is well known, all soft-pion results can be reproduced by calculating processes to lowest order using chiral Lagrangians. The success of soft-pion theorems in explaining the intermediate range part of the two-nucleon potential suggests that one should employ pv-coupling rather than ps-coupling. (The use of ps-coupling requires that one considers complicated nonlinear pion-sigma coupling terms.)

The OBEP generated by the exchange of s-, ps- and v-bosons can be written in the form

$$V(q',q) = \sum_{\alpha=s,ps,v} F_{\alpha}^{Born}(q',q) \ , \qquad (1.3.7)$$

where

$$F_{\alpha}^{Born}(q',q) = \bar{u}(-q')\ \Gamma_{\alpha}\ u(-q)\ P_{\alpha}\ \bar{u}(q')\ \Gamma_{\alpha}\ u(q) \ , \qquad (1.3.8)$$

represents the Born term Feynman amplitudes. Here P_{α} are meson propagators and Γ_{α} are meson-nucleon vertices.

In order to construct the dynamical equations used to unitarize the OBEP, the potential must be modified by introducing form factors $F_{\alpha}(q',q)$. This essentially consists in replacing g_{α} by $g_{\alpha}F_{\alpha}(q',q)$ and insures convergence of various integrals. In the absence of form factors, the divergent behavior of the OBE amplitudes can be attributed to the fact that point-like nucleons are employed in the OBE model.

In the OBEP model, the masses and coupling constants are determined by a detailed fit to the two-nucleon data. The main difference among various potentials lies in the treatment of the

two-pion system and in the details of the mesonic coupling and the cut-off factors.

Information concerning masses, coupling constants and other quantum numbers of these mesons are listed in Table 1 and Table 2 for OBE potentials HEA and HM2.

Chapter 2

The Pseudoparticle Model

2.1 Introduction

The original Brueckner program required that one calculate the properties of nuclear matter and finite nuclei starting from the knowledge of the nucleon-nucleon interaction in free space. The use of the Dirac equation for the description of nucleon motion has led to important advances in this program. However, calculations of the properties of finite nuclei are very difficult unless one uses the Dirac-Hartree or Dirac-Hartree-Fock approximations. In Ref.3 and Ref.4 we constructed a (density-dependent) effective interaction which reproduces rather accurately the nucleon self-energy in nuclear matter and the Migdal parameters obtained via Relativistic-Brueckner-Hartree-Fock calculations. The saturation curves of various boson exchange potentials yielded the generally accepted values for the binding energy and saturation density of nuclear matter (Fig.2 and Fig.3). We also obtained quite reasonable values for the incompressibility parameter. (These values are quite similar to those obtained earlier

using the full RBHF analysis.-See Table 3).

The effective interaction is constructed by adding Born terms, describing the exchange of pseudoparticles, to the Born terms of the Dirac-Hartree-Fock analysis. For the one-boson-exchange potential (OBEP) HEA (Ref.7), we add three pseudoparticles, with coupling constants and masses as given in Table 1. For the potential HM2 (Ref.8) we add two pseudoparticles, with coupling constants and masses as given in Table 2. These two potentials differ mainly in the strength of the tensor force. Here, for simplicity, we have dropped the dependence of the coupling constants of the pseudoparticles on the density of the medium in our calculations of finite nuclei.

2.2 Relativistic-Brueckner-Hartree-Fock Theory and the Effectivė Interaction

The nucleon spinor in nuclear matter satisfies the Dirac equation (Ref.5)

$$[\ \vec{\alpha}\cdot\vec{p} + \beta m_N + \beta\ \Sigma(\vec{p},k_f,\{f\})\ ]\ f(\vec{p},s) = \epsilon(\vec{p})f(\vec{p},s)\ . \qquad (2.2.1)$$

Here Σ is the self-energy which depends on the spinors $f(\vec{p},s)$ and the density of the system.

$$\Sigma(\vec{p}) = \sum_s \int \frac{d\vec{q}}{(2\pi)^3}\left[\frac{m_N}{E_N(\vec{q})}\right]\langle \vec{p},\bar{f}(\vec{p},s)|\hat{M}(1-p_{12})|\vec{p},f(\vec{q},s)\rangle\ \theta(k_f-|\vec{q}|)\ . \tag{2.2.2}$$

We found it useful to introduce various matrix elements of self-energy (Ref.5). We have

$$\Sigma^{++}_{ss}(\vec{p}) = \sum_{s'} \int \frac{d\vec{q}}{(2\pi)^3}\left[\frac{m_N}{E_N(\vec{q})}\right]\langle \bar{u}(\vec{p},s)\bar{f}(\vec{q},s')|\hat{M}(1-p_{12})|u(\vec{p},s)f(\vec{q},s')\rangle \times\theta(k_f-|\vec{q}|)\ , \tag{2.2.3}$$

$$\Sigma^{-+}_{s',s}(\vec{p}) = \langle s'|\vec{\sigma}\cdot\vec{p}|s\rangle\Sigma^{-+}(\vec{p})\ , \tag{2.2.4}$$

$$\Sigma^{-+}(\vec{p}) = \sum_{s'} \int \frac{d\vec{q}}{(2\pi)^3}\left[\frac{m_N}{E_N(\vec{q})}\right]\langle \bar{w}(\vec{p},s)\bar{f}(\vec{q},s')|\hat{M}(1-p_{12})|u(\vec{p},s)f(\vec{q},s')\rangle \times\theta(k_f-|\vec{q}|)\ , \tag{2.2.5}$$

and

$$\Sigma^{--}_{ss}(\vec{p}) = \sum_{s'} \int \frac{d\vec{q}}{(2\pi)^3}\left[\frac{m_N}{E_N(\vec{q})}\right]\langle \overline{w}(\vec{p},s)\overline{f}(\vec{q},s')|\hat{M}(1-p_{12})|w(\vec{p},s)f(\vec{q},s')\rangle$$

$$\times\theta(k_f-|\vec{q}|) \quad . \qquad (2.2.6)$$

etc. In these equations $w(\vec{p},s) = v(-\vec{p},-s)$. The $u(\vec{p},s)$ and $v(\vec{p},s)$ are the Dirac spinors as defined by Bjorken and Drell (Ref.14). In these equations $\hat{M}$ is the reaction matrix and p_{12} is an exchange operator. The reaction matrix $\hat{M}$ satisfies an equation of the form (Ref.5)

$$\hat{M} = U + U\,\hat{g}\,\hat{M} \quad . \qquad (2.2.7)$$

The Hartree-Fock results for $\Sigma^{++}(\vec{p})$, etc., are obtained by replacing $\hat{M}$ by U in the above equations. The potential U describes the exchange of various "mesons" ($\sigma,\pi,\rho,\omega,\ldots$) which play a role in the boson-exchange model of nuclear forces.

The effective potential $v_{eff} = U + \Delta U$, when inserted into equations for Σ^{++}, etc., will reproduce the results obtained with the reaction matrix M.

For the one-boson-exchange potential (OBEP) HEA (Ref.7), we need

only introduce three pseudoparticles to reproduce various matrix elements of the reaction matrix. These are pseudo-sigma, pseudo-omega and pseudo-delta fields. One might think that a pseudo-pion would be required, but the exchange of pions, beyond the Born terms, gives rise to effects that can be readily simulated by sigma exchange. The coupling constants and masses of these pseudoparticles are given in Table 1. With reference to the potential HEA, we put

$$U_{eff} = U_{eff}^{(1)} + U_{eff}^{(2)} \quad . \tag{2.2.8}$$

where

$$U_{eff}^{(1)} = U = U_{\sigma} + U_{\omega} + U_{\rho} + U_{\pi} + U_{\eta} + U_{\phi} + U_{\delta} \quad , \tag{2.2.9}$$

and

$$U_{eff}^{(2)} = \Delta U = \Delta U_{\sigma} + \Delta U_{\omega} + \Delta U_{\delta} \quad . \tag{2.2.10}$$

For the potential HM2 (Ref.8) we add two pseudoparticles with coupling constants and masses as given in Table 2.

Therefore, in the quasiparticle model we will use the approxi-

mation

$$\Sigma(\vec{p}) = \sum_s \int \frac{d\vec{q}}{(2\pi)^3}\left[\frac{m_N}{E_N(\vec{q})}\right]\langle \vec{p},\bar{f}(\vec{p},s)|(U+\Delta U)(1-p_{12})|\vec{p},f(\vec{q},s)\rangle\ \theta(k_f-|\vec{q}|)\ . \tag{2.2.11}$$

Chapter 3

Translationally-Invariant Relativistic Mean-Field Theory

3.1 The Self-Energy of Finite Nuclei

In ref. 5 we presented the following equation for the nucleon wave function, which has its origin in the mean-field dynamics exhibited in Fig. 4a,

$$[\ \gamma^0\ [\ W - E_{A-1}(\vec{P}-\vec{k})\ ] - \vec{\gamma}\cdot(\vec{P}-\vec{k}) - m_N\ ]\ (\vec{k}|\psi_{\vec{P}})$$

$$= \int d\vec{k}'\ (\vec{k}|\Sigma(W)|\vec{k}')\ (\vec{k}'|\psi_{\vec{P}})\ . \qquad (3.1.1)$$

We will take $\vec{P} = 0$ and put $E_{A-1}(\vec{k}) = [\ M_{A-1}^{\ 2} + \vec{k}^2\ ]^{1/2}$. Here M_{A-1} is the mass of the residual system of (A-1) nucleons. In the rest frame of the A-body system ($\vec{P} = 0$) we also have $W = M_A$. (In general, $W = [P^2 + M_A^2]^{1/2}$).

It is useful to consider an A-body system with total angular momentum equal to zero, so that we can label the residual system by

the angular momenta of the hole state, ljm. Therefore the wave function, $(\vec{k}|\psi_{\vec{P}})$ can be written as $\psi^{ljm}(\vec{k})$, when $\vec{P} = 0$.

In order to construct the self-energy, $\langle\vec{k}|\Sigma(W)|\vec{k}'\rangle = \Sigma(k,k',\cos\theta)$, we use the approximation shown in Fig. 4. In our earlier work we calculated Σ making use of the RBHF reaction matrices for nuclear matter. Here we use our effective interaction to evaluate the diagrams of Fig. 4c. (We remind the reader that Σ is a Dirac matrix.)

Let m denote the mass of the exchanged meson (or pseudoparticle), G denote the corresponding propagator and Γ denote the isospin-independent part of the nucleon-meson vertex.

We find that for the exchange of an isoscalar meson, for the <u>direct</u> diagram (See Fig.4c)

$$\Sigma = F^2[(k-k')^2]\ \Gamma(k-k')\int\frac{d\vec{Q}}{(2\pi)^3}(1/2)\mathrm{Tr}\{\rho(\vec{Q}',\vec{Q}'')\Gamma(k-k')\}G(k-k')\ , \qquad (3.1.2)$$

while for the <u>exchange</u> diagram

$$\Sigma = F^2[(k+k'+Q)^2] \int \frac{d\vec{Q}}{(2\pi)^3} \Gamma(k+k'+Q)\rho(\vec{Q}',\vec{Q}'')\Gamma(k+k'+Q)G(k+k'+Q) \ . \tag{3.1.3}$$

For the exchange of an isovector meson, we have for the <u>direct</u> diagram

$$\Sigma = 0 \ , \tag{3.1.4}$$

and for the <u>exchange</u> diagram

$$\Sigma = -3\ F^2[(k+k'+Q)^2] \int \frac{d\vec{Q}}{(2\pi)^3} \Gamma(k+k'+Q)\rho(\vec{Q}',\vec{Q}'')\Gamma(k+k'+Q)G(k+k'+Q) \ . \tag{3.1.5}$$

where $F[(k-k')^2]$ is a meson-nucleon vertex cut-off factor which appears in OBEP models, and which will be described more fully at a later point.

The quantity $\Gamma(k-k')$ is the meson-nucleon vertex. For the pion we used pseudovector coupling, since pseudoscalar pion coupling is untenable in a relativistic many-body theory unless additional

(chiral) constraints are imposed (Ref.5). Thus the pion-nucleon vertex is

$$\Gamma_\pi(q) = g_{pv}^{\pi}\, \gamma^5\, \not{q} \ . \qquad (3.1.6)$$

(Note that we have suppressed reference to isospin.)

For the rho-meson, we have

$$\Gamma^\mu(q) = g_\rho \left[\gamma^\mu + \frac{1}{2m_N} \frac{f_\rho}{g_\rho}\, i\sigma^{\mu\nu} q_\nu \right] , \qquad (3.1.7)$$

etc.

Further, we have used the definitions

$$\vec{Q}' = -\vec{Q} - \left[\frac{A-1}{A}\right] \vec{k}' \ , \qquad (3.1.8)$$

$$\vec{Q}'' = -\vec{Q} - \left[\frac{A-1}{A}\right] \vec{k} \ . \qquad (3.1.9)$$

The density matrix is given in terms of these momenta as (Ref.5)

$$\rho(\vec{Q}',\vec{Q}'') = \sum_{lj} \rho_{lj}(\vec{Q}',\vec{Q}'')$$

$$= \sum_{ljm} \psi^{ljm}(-\vec{k}'-\vec{Q},\vec{Q})\bar{\psi}^{ljm}(-\vec{k}-\vec{Q},\vec{Q}) \quad . \qquad (3.1.10)$$

(Note that ρ is a 4x4 Dirac matrix.)

One can perform the integral over $\vec{Q}$, the momentum of the (A-2)-body spectator, to define a form factor of the (A-1)-body system

$$\mathfrak{F}_{scalar}(q^2) = Tr \int d\vec{Q}\ \rho(\vec{Q}',\vec{Q}'') \quad . \qquad (3.1.11)$$

Once we have a set of wave functions, we can calculate the density matrix. Then knowledge of the interaction allows us to construct $\Sigma(k,k',\cos\theta)$. The general form of that quantity was given in Ref.5 as

$$\Sigma(k,k',\cos\theta) = A(k,k',\cos\theta) + \gamma^0 B(k,k',\cos\theta)$$

$$+ \frac{\vec{\gamma}\cdot(\vec{k}+\vec{k}')}{2m_N} C(k,k',\cos\theta)$$

$$+ i\,\frac{\vec{\gamma}\cdot(\vec{k}-\vec{k}')}{m_N} D(k,k',\cos\theta)$$

$$- \gamma^0\,\frac{\vec{\gamma}\cdot(\vec{k}-\vec{k}')}{2m_N} E(k,k',\cos\theta)$$

$$- i\gamma^0 \frac{\vec{\gamma}\cdot(\vec{k}+\vec{k}')}{2m_N} F(k,k',\cos\theta)$$

$$+ i \frac{\vec{\Sigma}\cdot(\vec{k}\times\vec{k}')}{m_N^2} G(k,k',\cos\theta)$$

$$- i\gamma^0 \frac{\vec{\Sigma}\cdot(\vec{k}\times\vec{k}')}{m_N^2} H(k,k',\cos\theta) \ , \qquad (3.1.12)$$

where we use the notation

$$\vec{\Sigma} = \begin{pmatrix} \vec{\sigma} & 0 \\ 0 & \vec{\sigma} \end{pmatrix} \ . \qquad (3.1.13)$$

In the OBEP model, form factors must be imposed on the potential to regularize divergences which appear when integrating over large momenta. Somehow, these form factors take into account the extended structure of the nucleon. For the potential HEA, the cut-off for scalar and pseudoscalar mesons is of the form

$$[\Lambda^2/(\Lambda^2-\Delta^2)]^2 \ , \qquad (3.1.14)$$

while for the vector mesons we use the cut-off factor

$$[\Lambda^2/(\Lambda^2-\Delta^2)]^2\bullet(\Lambda_v^2-m_v^2)/(\Lambda_v^2-\Delta^2) \quad . \qquad (3.1.15)$$

Here Δ^2 is the square of the four-momentum transfer and

$$\Lambda = 1950 \text{ MeV} \quad , \qquad (3.1.16)$$

$$\Lambda_v = 1250 \text{ MeV} \quad . \qquad (3.1.17)$$

For the potential HM2 one uses eikonal form factors. (See Appendix A.) Compared to the cut-off procedure for HEA, the eikonal treatment has several advantages:

(i) it can be theoretically motivated;

(ii) it strongly correlates the electromagnetic and the strong nucleon form factors;

(iii) it makes possible the use of meson parameters which are closer to the empirical values.

After we construct $\Sigma(k,k',\cos\theta)$, we can find $A(k',k,\cos\theta)$, $B(k',k,\cos\theta),\ldots,$ $H(k',k,\cos\theta)$ by taking traces. We can then compare our results with Dirac phenomenology.

3.2 Integral Equation for Nucleon Wave Functions

We can write the wave functions $\psi^{ljm}(\vec{k})$ as

$$\psi^{ljm}(\vec{k}) = \begin{pmatrix} R_U^{lj}(k)\, \mathcal{Y}^{ljm}(\hat{k}) \\ R_L^{\bar{l}j}(k)\vec{\sigma}\cdot\hat{k}\, \mathcal{Y}^{ljm}(\hat{k}) \end{pmatrix} , \qquad (3.2.1)$$

where

$$\bar{l} = \begin{cases} j + \frac{1}{2} \; ; & (l = j - \frac{1}{2}) \\ j - \frac{1}{2} \; ; & (l = j + \frac{1}{2}) \end{cases} . \qquad (3.2.2)$$

Substituting this into equation (3.1.1) we can obtain an equation for the radial wave functions

$$\left\{ \left[W - E_{A-1}^{lj}(\vec{k}) \right] \mathbb{I} - \begin{pmatrix} m_N & k \\ k & -m_N \end{pmatrix} \right\} \begin{pmatrix} R_U^{lj}(k) \\ R_L^{\bar{l}j}(k) \end{pmatrix}$$

$$= \int dk' k'^2 \begin{pmatrix} v_{11}^{l\bar{l}}(k,k') & v_{12}^{l\bar{l}}(k,k') \\ v_{21}^{l\bar{l}}(k,k') & v_{22}^{l\bar{l}}(k,k') \end{pmatrix} \begin{pmatrix} R_U^{lj}(k') \\ R_L^{\bar{l}j}(k') \end{pmatrix} , \qquad (3.2.3)$$

where the v's are constructed from the knowledge of

$$v(k,k',\cos\theta) = \gamma^0 \, \Sigma(k,k',\cos\theta) \tag{3.2.4}$$

That quantity has the following expansion

$$v_{11}(k,k',\cos\theta) = \sum_{ljm} v_{11}^{l\bar{l}}(k,k') \mathcal{Y}^{ljm}(\hat{k}) \mathcal{Y}^{ljm+}(\hat{k}') \ , \tag{3.2.5}$$

$$v_{12}(k,k',\cos\theta) = \sum_{ljm} v_{12}^{l\bar{l}}(k,k') \mathcal{Y}^{ljm}(\hat{k}) \mathcal{Y}^{\bar{l}jm+}(\hat{k}') \ , \tag{3.2.6}$$

$$v_{21}(k,k',\cos\theta) = \sum_{ljm} v_{21}^{l\bar{l}}(k,k') \mathcal{Y}^{\bar{l}jm}(\hat{k}) \mathcal{Y}^{ljm+}(\hat{k}') \ , \tag{3.2.7}$$

$$v_{22}(k,k',\cos\theta) = \sum_{ljm} v_{22}^{l\bar{l}}(k,k') \mathcal{Y}^{\bar{l}jm}(\hat{k}) \mathcal{Y}^{\bar{l}jm+}(\hat{k}') \ . \tag{3.2.8}$$

These expressions follow naturally after one chooses to write the wave function as in equation (3.2.1). Note that

$$W - E_{A-1}^{lj}(\vec{k}) = M_A - \left[\, (M_{A-1}^{lj})^2 + \vec{k}^2 \, \right]^{1/2} \tag{3.2.9}$$

$$\approx M_A - M_{A-1}^{lj} - \frac{\vec{k}^2}{2M_{A-1}^{lj}} + \frac{\vec{k}^4}{8(M_{A-1}^{lj})^3} + \ldots \tag{3.2.10}$$

$$\approx m_N - \epsilon^{lj} - \frac{\vec{k}^2}{2M_{A-1}^{lj}} + \frac{\vec{k}^4}{8(M_{A-1}^{lj})^3} + \ldots \quad . \qquad (3.2.11)$$

We see that ϵ^{lj} is the separation energy for the orbital lj. Thus equation (3.2.3) is an eigenvalue equation for the eigenvalue ϵ^{lj} and the eigenfunctions, $R_U^{lj}(k)$ and $R_L^{lj}(k)$. The potentials $v^{l\bar{l}}$ are functionals of these wave functions and, therefore, our equations require a self-consistent solution. To begin the iteration procedure, we use harmonic-oscillator wave functions as trial wave functions for the upper part of the wave function, $R_U^{lj}(k)$, while for the lower part we use $R_L^{lj}(k) = (k/2m_N)R_U^{lj}(k)$. Since the iteration converges, we find that the final result does not depend on the trial wave functions.

Chapter 4

Calculation of the Properties of Finite Nuclei

4.1 The Charge Density Distribution

In addition to the separation energies and the wave functions of each orbital, we have calculated the charge density distributions.(We use the formalism presented in Ref.6.) We can define a matter form factor, $F(q^2)$, for point-like nucleons, in terms of the electromagnetic current of such objects:

$$(\vec{p}'|J_\mu(0)|\vec{p}) = \frac{e(p_\mu + p'_\mu)}{(2\pi)^3[2E_N(\vec{p})2E_N(\vec{p}')]^{1/2}} F(q^2) \quad . \tag{4.1.1}$$

We may then define a charge form factor,

$$F_{ch}(q^2) = F(q^2)\ G_E^p(q^2) \quad , \tag{4.1.2}$$

with

$$G_E^p(q^2) = (1 - q^2/0.71)^{-2} \quad . \tag{4.1.3}$$

Here q^2 is in units of $(GeV)^2$. We have

$$\rho_{ch}(r) = Z \int \frac{d\vec{q}}{(2\pi)^3} e^{i\vec{q}\cdot\vec{r}} F_{ch}(q^2) , \qquad (4.1.4)$$

$$= \frac{Z}{2\pi^2 r} \int dq\, q\, \sin qr\, F_{ch}(q^2) . \qquad (4.1.5)$$

From the knowledge of $F_{ch}(q^2)$, we can calculate the charge radius:

$$\langle r^2 \rangle_{ch} = - 6 \left[\frac{dF_{ch}(q^2)}{dq^2} \right]_{q^2 = 0} . \qquad (4.1.6)$$

4.2 The Binding Energy of Finite Nuclei

For the binding energy we have (Ref.5)

$$B.E. = m_N A - \sum_{ljm} \int d\vec{p}\, \bar{\psi}^{ljm}(\vec{p}) \left(\vec{\gamma}\cdot\vec{p} + m_N \right) \psi^{ljm}(\vec{p})$$

$$- \frac{1}{2} \sum_{ljm} \int d\vec{p} \int d\vec{p}' \bar{\psi}^{ljm}(\vec{p}) \left(\vec{p}|\Sigma(W)|\vec{p}'\right) \psi^{ljm}(\vec{p}') , \qquad (4.2.1)$$

where we have again suppressed reference to isospin. The last equation may also be written as

$$B.E. = m_N A - \frac{1}{2}\sum_{ljm}\int d\vec{p}\ \bar{\psi}^{ljm}(\vec{p})\ [\ \vec{\gamma}\cdot\vec{p} + m_N + \gamma^0\epsilon^{lj}(\vec{p})\ ]\ \psi^{ljm}(\vec{p})\ , \tag{4.2.2}$$

where we have made use of Eq. (3.1.1). Here

$$\epsilon^{lj}(\vec{p}) = W - E_{A-1}^{lj}(\vec{p})\ . \tag{4.2.3}$$

Finally, we remark that the normalization condition is

$$\int d\vec{p}\ \psi^{ljm+}(\vec{p})\psi^{ljm}(\vec{p}) = 1\ , \tag{4.2.4}$$

or

$$\int dp\ p^2\ \left[(R_U^{lj}(p))^2 + (R_L^{lj}(p))^2\right] = 1\ . \tag{4.2.5}$$

Chapter 5

Results of Numerical Calculations

5.1 Separation Energies, Charge Radii and Binding Energies

Our results are presented in a series of tables and figures. In Tables 4 to 7 we present nucleon separation energies, root-mean-square radii and the binding energies per nucleon for ^{16}O and ^{40}Ca. We note that ^{16}O is underbound by 4 MeV and ^{40}Ca is underbound by about 3.5 MeV for the interaction HM2. (The results for the potential HEA presented in Tables 6 and 7 are quite unsatisfactory, as is the fit to the charge distribution for that interaction.)

We have also considered an arbitrary modification of the parameters of the effective interaction such that nuclear matter saturation is achieved at the conventionally accepted values for the binding energy and saturation density (Ref.4). The results for an interaction based upon such a procedure are given in the right-hand columns in Tables 4 to 7. It can be seen that the only gain is a small increase in the binding energies at the expense of a worse fit to the

charge radii. We do not recommend the use of the modified form of the interaction constructed in Ref. 4.

In Table 8 and 9 we present some of the results of a calculation of the properties of ^{16}O made by Muther, Machleidt and Brockman. Here RBHF denotes results of the renormalized Brueckner-Hartree-Fock theory. [To avoid confusion we have used the designation DBHF for the Dirac-Brueckner-Hartree-Fock theory, which is the relativistic version of the BHF theory. The parameter C refers to the magnitude of the shift of the particle spectrum away from the free spectrum (Ref.2). Results are also given for the case C = 0 in Ref. 2]. It is interesting to note, that while our result for the binding energy for the potential HM2 (3.89 MeV) is less satisfactory than the result for the interaction used in Ref. 2 (6.42 MeV), our result for the r.m.s. radius (2.74 fm) is superior to the result given in Ref. 2 (2.464 fm or 2.479 fm). We are not able to understand the origin of these differences, since we are comparing results for different potentials and for different calculational methods. Ideally, different potentials should be compared using the same computational methods; however, that has not been done at this time.

5.2 Wave Functions in Momentum-Space and Coordinate-Space

In Figs. 5 and 6 we present coordinate-space wave functions obtained for ^{16}O and ^{40}Ca. Here we have transformed our momentum-space wave functions to coordinate space, since the coordinate-space wave functions have a more familiar appearance. Both the upper and lower components, $R_U^{lj}(r)$ and $R_L^{lj}(r)$, are shown in figures. [We should remind the reader that these wave functions describe the relative motion of the nucleon and the (A-1)-body system.(Ref. 9)] The wave functions can be used to calculate various physical quantities.

In Figs. 7 and 8 we present the momentum-space wave functions obtained for ^{16}O and ^{40}Ca.

5.3 Potentials $A(k,k',\cos\theta), B(k,k',\cos\theta), \ldots, H(k,k',\cos\theta)$

We calculated A,B,...,H for different values of k, k', $\cos\theta$. In Figs. 9 to 13 we present contour plots of the functions $A(k,k',\cos\theta)$, $B(k,k',\cos\theta)$, $C(k,k',\cos\theta)$, $E(k,k',\cos\theta)$ and $H(k,k',\cos\theta)$ for the case

$\theta = 0$. (We have found that $D(k,k',\cos\theta)$ and $F(k,k',\cos\theta)$ are very small for all values of k, k' and $\cos\theta$; $G(k,k',\cos\theta)$ is also quite small except for some small regions.) As expected from studies of nuclear matter, A and B are the most important potentials, while C plays a significant, but somewhat less important role.

5.4 Charge Density Distributions

We calculated the charge distribution, both in momentum space and in coordinate space, for ^{16}O and ^{40}Ca. In Figs. 14 and 15 we show the charge distributions we have obtained when using the effective interaction based upon the potential HM2. In these figures the solid lines and the shaded regions denote the experimental data. The dash-dot line is our result, which in the case of ^{16}O reproduces the experimental data closely, so that the solid and dash-dot lines are indistinguishable in the figure for $r > 1$ fm. The dashed line is the result of Horowitz and Serot (Ref. 10) obtained some years ago. (In their work the interaction was adjusted to give the correct root-mean-square radius for ^{40}Ca and, therefore, one sees a quite good fit to the data in Fig. 15. More recent work using more elaborate versions of

the Walecka model, which have additional parameters, can provide good fits to the ground state properties of nuclei across the periodic table.)

Chapter 6

Concluding Remarks

Our goal in this work has been to apply the effective interaction, which was constructed in earlier work, in a Dirac-Hartree-Fock calculation of finite nuclei (Ref.3). (Note that, once the interaction is constructed, there are no free parameters in our calculation.) We found that the effective interaction provides a good description of the charge density of ^{16}O and ^{40}Ca. Reasonable results are obtained for separation energies; however, these nuclei are somewhat underbound. In part, this reflects the fact that the one-boson-exchange potentials used here also underbind nuclear matter to some degree. For simplicity, we have dropped the dependence of the coupling constants of the pseudoparticles on the density of the medium. From Ref. 4, we know that approximation also causes some degree of underbinding.

One satisfactory features of the relativistic quasiparticle method is that the interaction we have constructed describes the full complexity of the spin and isospin dependence of the nucleon-nucleon interaction. Therefore, as we have seen in earlier work, we are able

to make a successful calculation of the Migdal parameters of the nucleon-nucleon interaction (Refs.3,5). One might contemplate going beyond the approximations used here and consider the admixture into the ground state of low-lying two-particle two-hole excitations; however, we have not undertaken that program.

We tried to use our method to calculate the properties of heavy nuclei such as ^{208}Pb. However, due to the limitation of computer time, we did not have enough points for the radial wave functions of 2, 3 or more nodes. Therefore we were not able to obtain satisfactory results.

We made the approximation that the atomic number of the nucleus is rather large so we could neglect the difference between the amplitudes of an A-particle system and the amplitudes of an (A-1)-particle system. However, for ^{16}O, A is only 16. The deviation of the theoretical result from the experimental one is what one might expect. Considering that we obtain the energy levels and the binding energy mainly from the difference of two very large potentials, A and B, and that we did not introduce any free parameters, the results presented here are quite satisfactory.

Appendix A

Eikonal Form Factor[8]

In this Appendix we give the eikonal form factor used for the potential HM2. The eikonal form factor is denoted as $F_i(t,u|q_0^2)$, where $i = \sigma,\omega,\rho,\pi$...."mesons". We have

$$F_i(t,u|q_0^2) = \exp\left[2i\{ [\chi(t)-\chi(m_i^2)] + [\chi(u)-\chi(4m_N^2-s-m_i^2)] \}\right] , \quad (A.1)$$

where

$$t = (E_q, - E_q)^2 - (\vec{q}' - \vec{q})^2 , \quad (A.2)$$

$$u = (E_q, - E_q)^2 - (\vec{q}' + \vec{q})^2 , \quad (A.3)$$

$$E_q^2 = m_N^2 + \vec{q}^2 . \quad (A.4)$$

The starting energy (Ref.8) is

$$s = (E_q, + E_q)^2 - (\vec{q}' + \vec{q})^2 , \quad (A.5)$$

and

$$
i\chi(y) = \begin{cases} -2\gamma \dfrac{2m_N^2 - y}{\sqrt{y(4m_N^2 - y)}} \arctan \sqrt{\dfrac{y}{(4m_N^2 - y)}} \\ \qquad (0 < y < 4m_N^2) \\ -2\gamma \dfrac{2m_N^2 - y}{\sqrt{-y(4m_N^2 - y)}} \ln \left[\sqrt{-y/(4m_N^2)} + \sqrt{1 - y/(4m_N^2)} \right] . \\ \qquad (y < 0) \end{cases} \tag{A.6}
$$

Appendix B

Partial Wave Expansion of the Self-Energy

Recall that we had written

$$v(k,k',\cos\theta) = \gamma^0 \, \Sigma(k,k',\cos\theta) \ . \tag{B.1}$$

We now put

$$v(k,k',\cos\theta) = \begin{pmatrix} v_{11} & v_{12} \\ v_{21} & v_{22} \end{pmatrix} \ , \tag{B.2}$$

and develop equations for $v_{11}(k,k',\cos\theta)$, $v_{12}(k,k',\cos\theta)$, etc.

We can show that the v's can be written as follows

$$v_{11}(k,k',\cos\theta) = v_{11}^{a} \, \mathbb{I} + \vec{\sigma}\cdot\hat{k} \, v_{11}^{b} \, \vec{\sigma}\cdot\hat{k}' \ , \tag{B.3}$$

$$v_{12}(k,k',\cos\theta) = \vec{\sigma}\cdot\hat{k} \, v_{12}^{a} + v_{12}^{b} \, \vec{\sigma}\cdot\hat{k}' \ , \tag{B.4}$$

$$v_{21}(k,k',\cos\theta) = \vec{\sigma}\cdot\hat{k} \, v_{21}^{a} + v_{21}^{b} \, \vec{\sigma}\cdot\hat{k}' \ , \tag{B.5}$$

$$v_{22}(k,k',\cos\theta) = v_{22}^{a}\,\mathbb{I} + \vec{\sigma}\cdot\hat{k}\; v_{22}^{b}\;\vec{\sigma}\cdot\hat{k}' \quad , \tag{B.6}$$

where

$$v_{11}^{a}(k,k',\cos\theta) = A + B - \frac{\vec{k}\cdot\vec{k}'}{m_N^2}\,(G - H) \quad , \tag{B.7}$$

$$v_{11}^{b}(k,k',\cos\theta) = \frac{kk'}{m_N^2}\,(G - H) \quad , \tag{B.8}$$

$$v_{12}^{a}(k,k',\cos\theta) = \frac{k}{2m_N}\,(C + 2iD - E - iF) \quad , \tag{B.9}$$

$$v_{12}^{b}(k,k',\cos\theta) = \frac{k'}{2m_N}\,(C - 2iD + E - iF) \quad , \tag{B.10}$$

$$v_{21}^{a}(k,k',\cos\theta) = \frac{k}{2m_N}\,(C + 2iD + E + iF) \quad , \tag{B.11}$$

$$v_{21}^{b}(k,k',\cos\theta) = \frac{k'}{2m_N}\,(C - 2iD + E - iF) \quad , \tag{B.12}$$

$$v_{22}^{a}(k,k',\cos\theta) = - A + B + \frac{\vec{k}\cdot\vec{k}'}{m_N^2}\,(G + H) \quad , \tag{B.13}$$

$$v_{22}^{b}(k,k',\cos\theta) = - \frac{kk'}{m_N^2}\,(G + H) \quad , \tag{B.14}$$

We can also perform a partial-wave analysis. If we use the expansion

$$v_{11}^{a}(k,k',\cos\theta) = \sum_{ljm} v_{11}^{al}(k,k')\, \mathcal{Y}^{ljm}(\hat{k})\, \mathcal{Y}^{ljm+}(\hat{k}') \ , \qquad \text{(B.15)}$$

$$v_{11}^{b}(k,k',\cos\theta) = \sum_{ljm} v_{11}^{bl}(k,k')\, \mathcal{Y}^{ljm}(\hat{k})\, \mathcal{Y}^{ljm+}(\hat{k}') \ , \qquad \text{(B.16)}$$

we have

$$v_{11}(k,k',\cos\theta) = \sum_{ljm} v_{11}^{l\bar{1}}(k,k')\, \mathcal{Y}^{ljm}(\hat{k})\, \mathcal{Y}^{ljm+}(\hat{k}') \ , \qquad \text{(B.17)}$$

where

$$v_{11}^{l\bar{1}}(k,k') = v_{11}^{al}(k,k') + v_{11}^{b\bar{1}}(k,k') \ . \qquad \text{(B.18)}$$

Similarly, if we use the expansion

$$v_{12}^{a}(k,k',\cos\theta) = \sum_{ljm} v_{12}^{al}(k,k')\, \mathcal{Y}^{ljm}(\hat{k})\, \mathcal{Y}^{ljm+}(\hat{k}') \ , \qquad \text{(B.19)}$$

$$v_{12}^{b}(k,k',\cos\theta) = \sum_{ljm} v_{12}^{bl}(k,k')\, \mathcal{Y}^{ljm}(\hat{k})\, \mathcal{Y}^{ljm+}(\hat{k}') \ . \qquad \text{(B.20)}$$

we find

$$v_{12}(k,k',\cos\theta) = -\sum_{ljm} v_{12}^{l\bar{l}}(k,k')\, \mathcal{Y}^{ljm}(\hat{k})\, \mathcal{Y}^{\bar{l}jm+}(\hat{k}') \ , \qquad (B.21)$$

where

$$v_{12}^{l\bar{l}}(k,k') = v_{12}^{a\bar{l}}(k,k') + v_{12}^{bl}(k,k') \ . \qquad (B.22)$$

Also

$$v_{21}^{a}(k,k',\cos\theta) = \sum_{ljm} v_{21}^{al}(k,k')\, \mathcal{Y}^{ljm}(\hat{k})\, \mathcal{Y}^{ljm+}(\hat{k}') \ , \qquad (B.23)$$

$$v_{21}^{b}(k,k',\cos\theta) = \sum_{ljm} v_{21}^{bl}(k,k')\, \mathcal{Y}^{ljm}(\hat{k})\, \mathcal{Y}^{ljm+}(\hat{k}') \ . \qquad (B.24)$$

$$v_{21}(k,k',\cos\theta) = -\sum_{ljm} v_{21}^{l\bar{l}}(k,k')\, \mathcal{Y}^{\bar{l}jm}(\hat{k})\, \mathcal{Y}^{ljm+}(\hat{k}') \ , \qquad (B.25)$$

$$v_{21}^{l\bar{l}}(k,k') = v_{21}^{al}(k,k') + v_{21}^{b\bar{l}}(k,k') \ . \qquad (B.26)$$

$$v_{22}^{a}(k,k',\cos\theta) = \sum_{ljm} v_{22}^{al}(k,k')\, \mathcal{Y}^{ljm}(\hat{k})\, \mathcal{Y}^{ljm+}(\hat{k}') \ , \qquad (B.27)$$

$$v_{22}^{b}(k,k',\cos\theta) = \sum_{ljm} v_{22}^{bl}(k,k')\, \mathcal{Y}^{ljm}(\hat{k})\, \mathcal{Y}^{ljm+}(\hat{k}') \ . \qquad (B.28)$$

$$v_{22}(k,k',\cos\theta) = \sum_{ljm} v_{22}^{l\bar{l}}(k,k')\, \mathcal{Y}^{\bar{l}jm}(\hat{k})\, \mathcal{Y}^{\bar{l}jm+}(\hat{k}') \ , \qquad (B.29)$$

$$v_{22}^{l\bar{l}}(k,k') = v_{22}^{a\bar{l}}(k,k') + v_{22}^{bl}(k,k') \quad . \tag{B.30}$$

If we also expand A, B, ..., H as

$$A(k,k',\cos\theta) = \sum_{ljm} A_l(k,k')\, \mathcal{Y}^{ljm}(\hat{k})\, \mathcal{Y}^{ljm+}(\hat{k}') \quad , \tag{B.31}$$

$$= \sum_{lm} A_l(k,k')\, Y_{lm}(\hat{k})\, Y_{lm}^{*}(\hat{k}') \quad , \tag{B.32}$$

$$= \sum_{l} \frac{(2l+1)}{4\pi} A_l(k,k')\, P_l(\cos\theta) \quad , \tag{B.33}$$

etc., we can find relations among the $v^{l\bar{l}}(k,k')$ and the potentials $A_l(k,k')$, $B_l(k,k')$,..., etc. We have

$$v_{11}^{l\bar{l}}(k,k') = A_l(k,k') + B_l(k,k')$$

$$- \frac{kk'}{m_N^2} \left\{ \frac{l+1}{2l+1} \left[G_{l+1}(k,k') - H_{l+1}(k,k') \right] \right.$$

$$+ \frac{l+1}{2l+1} \left[G_{l-1}(k,k') - H_{l-1}(k,k') \right]$$

$$\left. - \left[G_{\bar{l}}(k,k') - H_{\bar{l}}(k,k') \right] \right\} \quad , \tag{B.34}$$

$$v_{12}^{l\bar{l}}(k,k') = \frac{k'}{2m_N}\left[C_{\bar{l}} + 2iD_{\bar{l}} - E_{\bar{l}} - iF_{\bar{l}} \right]$$

$$+ \frac{k}{2m_N}\left[C_l - 2iD_l + E_l - iF_l \right] , \qquad (B.35)$$

$$v_{21}^{l\bar{l}}(k,k') = \frac{k'}{2m_N}\left[C_l + 2iD_l + E_l + iF_l \right]$$

$$+ \frac{k}{2m_N}\left[C_{\bar{l}} - 2iD_{\bar{l}} - E_{\bar{l}} + iF_{\bar{l}} \right] , \qquad (B.36)$$

and

$$v_{22}^{l\bar{l}}(k,k') = - A_{\bar{l}} + B_{\bar{l}} + \frac{kk'}{m_N^2}\left\{ \frac{\bar{l}+1}{2\bar{l}+1}\left[G_{\bar{l}+1} + H_{\bar{l}+1} \right] \right.$$

$$\left. + \frac{\bar{l}}{2\bar{l}+1}\left[G_{\bar{l}-1} + H_{\bar{l}-1} \right] - \left[G_l + H_l \right] \right\} . \qquad (B.37)$$

Appendix C

Harmonic-Oscillator Radial Functions and Generalized Spherical Harmonics

We used the harmonic-oscillator functions as trial wave functions for the radial part of our wave functions. These are normalized to unity:

$$\int_0^\infty R^2(r) r^2 dr = 1 \ . \tag{C.1}$$

They may be written

$$R_{nl}(r) = \pi^{-1/4} \alpha^{3/2} \left[\frac{2^{l-n+3} \ (2l+2n-1)!!}{[(2l+1)!!]^2 \ (n-1)!} \right]^{1/2} (\alpha r)^l e^{-1/2(\alpha r)^2}$$

$$\times \sum_{k=0}^{n-1} (-1)^k \ 2^k \ \frac{(n-1)!(2l+1)!!}{(n-1-k)!k!(2l+2k+1)!!} \ (\alpha^2 r^2)^k \ , \tag{C.2}$$

in a notation where the lowest oscillator state has principal quantum number n = 1, and

$$\alpha \equiv (M\omega/\hbar)^{1/2} \tag{C.3}$$

is the oscillator range parameter for an oscillator of angular frequency ω. The energy of the oscillator is

$$E_{nl} = \hbar\omega\{2(n-1) + l + 3/2\} . \qquad (C.4)$$

Some particular examples of these radial functions are

$$R_{1l}(r) = \pi^{-1/4}\,\alpha^{3/2}\left[\frac{2^{l+2}}{(2l+1)!!}\right]^{1/2}(\alpha r)^{l} e^{-1/2(\alpha r)^2} , \qquad (C.5)$$

$$R_{2l}(r) = \pi^{-1/4}\,\alpha^{3/2}\left[\frac{2^{l+3}}{(2l+3)!!}\right]^{1/2}(\alpha r)^{l} e^{-1/2(\alpha r)^2} \times[(2l+3)/2 - (\alpha r)^2] , \qquad (C.6)$$

$$R_{3l}(r) = \pi^{-1/4}\,\alpha^{3/2}\left[\frac{2^{l+3}}{(2l+5)!!}\right]^{1/2}(\alpha r)^{l} e^{-1/2(\alpha r)^2} \times[(2l+3)(2l+5)/4 - (2l+5)(\alpha r)^2 + (\alpha r)^4] . \qquad (C.7)$$

We used the generalized spherical harmonics defined by

$$\mathcal{Y}^{ljm}(\hat{k}) = \sum_{m_l} C^{l\ \frac{1}{2}\ j}_{m_l\ m_s\ m}\, Y_{lm_l}(\hat{k})\, \chi_{m_s} , \qquad (C.8)$$

where

$$C^{l\ \frac{1}{2}\ j}_{m_l\ m_s\ m}$$

is a Clebsch-Gordan coefficient, which, in this case, couples the orbital angular momentum l, carried by the spherical harmonic Y_{lm_l}, to spin 1/2, in order to obtain a function of good total angular momentum, j.

Table 1

HEA Potential

Coupling constants and meson masses for the potential HEA. Also presented are the coupling constants for the pseudoparticles for $k_F = k_F^{NM} = 1.36\ fm^{-1}$.

Meson	Isospin T	Spin Parity J^π	Mass (MeV)	Coupling Constant $(g^2/4\pi)$	f/g	Pseudoparticle Coupling Constants
σ	0	0^+	500.0	4.63	0.0	$\delta g_\sigma^2/(4\pi)=-2.81$ [a]
π	1	0^-	138.5	13.0	0.0	
ω	0	1^-	782.8	14.0	0.0	$\delta g_\omega^2/(4\pi)=14.2$ [b]
ϕ	0	1^-	1020.	7.00	0.0	
ρ	1	1	763.0	1.50	3.5	
δ	1	0^+	960.0	4.74	0.0	$\delta g_\delta^2/(4\pi)=5.54$ [c]
η	0	0^-	548.5	6.00	0.0	

a) The sign is such as to increase the attraction due to sigma exchange--see Ref.3. (M_σ = 1 GeV.)

b) The sign is such as to decrease the repulsion due to omega exchange. (M_ω = 1 GeV.)

c) The sign is such as to decrease the repulsion due to delta exchange. (M_δ = 1.25 GeV.)

Table 2

HM2 Potential

Coupling constants and meson masses for the potential HM2. Also presented are the coupling constants for the pseudoparticles for $k_F = k_F^{NM} = 1.36\ fm^{-1}$.

Meson	Isospin T	Spin Parity J^π	Mass (MeV)	Coupling Constant $(g^2/4\pi)$	f/g	Pseudoparticle Coupling Constants
σ	0	0^+	520.0	5.66	0.0	$\delta g_\sigma^2/(4\pi)=-1.15$ [a]
π	1	0^-	138.0	14.2	0.0	
ω	0	1^-	782.8	10.0	0.0	$\delta g_\omega^2/(4\pi)=6.52$ [b]
ρ	1	1^-	711.0	0.50	6.2	
δ	1	0^+	960.0	0.82	0.0	
η	0	0^-	548.5	2.00	0.0	

a) The sign is such as to increase the attraction in the sigma channel. We can put $\delta g_\sigma^2/(4\pi) = -1.15 = 4.34 - 5.49$, where the 4.34 represents the necessary reduction in the attraction due to correlations and -5.49 represents the increase in "sigma-like" attraction due to higher-order terms of pion-exchange dynamics- see Ref.3. (M_σ = 1 GeV.)

b) The sign is such as to decrease the repulsion due to omega exchange. (M_ω = 1 GeV.)

Table 3

Fermi momentum, k_F, at saturation and the incompressibility parameter, K_∞, calculated in the pseudoparticle method for the potential HM2. The coupling constants of the pseudoparticles are chosen to be either density-dependent or density-independent, as discussed in the Ref.4. (See Fig. 2 and 3.)

HM2	$k_F(fm^{-1})$	K_∞(MeV)	Pseudoparticle Parameters
Approximation 1	1.19	220	density-dependent
Approximation 2	1.37	260	density-independent

Table 4

HM2 Potential

The binding energy per particle, charge radius and separation energies for ^{16}O.

	Expt.	Unmodified Coupling Constants		Modified[a] Coupling Constants	
$\langle r^2 \rangle_{ch}^{1/2}$	2.73 fm	2.74 fm		2.67 fm	
B.E./A	7.98 MeV	3.89 MeV		4.67 MeV	
		Separation Energies (MeV)			
	n	n	p	n	p
$1s_{1/2}$	(40)	40.9	38.0	45.7	42.1
$1p_{3/2}$	21.8	15.8	13.5	18.3	15.3
$1p_{1/2}$	15.7	11.0	8.8	12.6	9.7

a) The interaction was modified to achieve the 'correct' binding energy for nuclear matter (Ref.4).

Table 5

HM2 Potential

The binding energy per particle, charge radius and separation energies for ^{40}Ca.

	Expt.	Unmodified Coupling Constants		Modified[a] Coupling Constants	
$\langle r^2 \rangle_{ch}^{1/2}$	3.48 fm	3.49 fm		3.42 fm	
B.E./A	8.45 MeV	4.96 MeV		6.26 MeV	
		Separation Energies (MeV)			
	n	n	p	n	p
$1s_{1/2}$		57.8	50.8	63.6	56.4
$1p_{3/2}$		37.6	30.7	41.7	34.6
$1p_{1/2}$		34.6	27.6	38.2	31.1
$1d_{5/2}$	22.6	18.1	12.3	20.7	14.6
$2s_{1/2}$	18.2	12.3	6.7	13.9	8.1
$1d_{3/2}$	15.6	12.7	6.8	14.4	8.4

a) See note for Table 4.

Table 6

HEA Potential

The binding energy per particle, charge radius and separation energies for ^{16}O.

	Expt.	Unmodified Coupling Constants		Modified[a] Coupling Constants	
$\langle r^2 \rangle_{ch}^{1/2}$	2.73 fm	2.98 fm		2.50 fm	
B.E./A	7.98 MeV	1.12 MeV		5.30 MeV	
		Separation Energies (MeV)			
	n	n	p	n	p
$1s_{1/2}$	(40)	23.9	21.9	45.8	43.0
$1p_{3/2}$	21.8	7.6	5.6	20.7	18.0
$1p_{1/2}$	15.7	4.6	2.8	10.7	8.2

a) See note for Table 4.

Table 7

HEA Potential

The binding energy per particle, charge radius and separation energies for ^{40}Ca.

	Expt.	Unmodified Coupling Constants		Modified[a] Coupling Constants	
$\langle r^2 \rangle_{ch}^{1/2}$	3.48 fm	3.68 fm		3.23 fm	
B.E./A	8.45 MeV	1.74 MeV		7.38 MeV	
		Separation Energies (MeV)			
	n	n	p	n	p
$1s_{1/2}$		39.8	34.4	60.8	54.6
$1p_{3/2}$		24.9	20.0	42.5	36.7
$1p_{1/2}$		22.3	17.3	37.3	31.3
$1d_{5/2}$	22.6	10.8	6.4	23.8	18.4
$2s_{1/2}$	18.2	7.9	3.6	13.3	7.9
$1d_{3/2}$	15.6	6.1	1.8	12.9	7.5

a) See note for Table 4.

Table 8

Results of calculations of the properties of ^{16}O made by Muther, Machleidt and Brockman (Ref. 2). [Here C is a parameter which specifies the particle-state spectrum and RBHF refers to either a renormalized Brueckner-Hartree-Fock calculation or a normalized DBHF calculation.]

Nonrelativistic Calculation			
	Expt.	BHF(C=0)	RBHF(C=8)
$<r^2>_{ch}^{1/2}$	(2.7±0.05) fm	2.295 fm	2.324 fm
B.E./A	7.98 MeV	5.71 MeV	6.67 MeV
$1s_{1/2}$	40±8 MeV	52.98 MeV	48.25 MeV
$1p_{3/2}$	18.4 MeV	24.31 MeV	21.55 MeV
$1p_{1/2}$	12.1 MeV	17.15 MeV	15.55 MeV

Table 9

Results of calculations of the properties of ^{16}O made by Muther, Machleidt and Brockman (Ref. 2). [Here C is a parameter which specifies the particle-state spectrum and RBHF refers to either a renormalized Brueckner-Hartree-Fock calculation or a normalized DBHF calculation.]

Relativistic Calculation (DBHF) Effective Density Approach			
	Expt.	BHF(C=0)	RBHF(C=8)
$<r^2>_{ch}^{1/2}$	(2.7±0.05) fm	2.464 fm	2.479 fm
B.E./A	7.98 MeV	5.65 MeV	6.42 MeV
$1s_{1/2}$	40±8 MeV	44.11 MeV	41.33 MeV
$1p_{3/2}$	18.4 MeV	19.79 MeV	18.03 MeV
$1p_{1/2}$	12.1 MeV	11.29 MeV	10.65 MeV

Figure Captions

Fig. 1:

Calculation of the self-energy in the relativistic quasiparticle method. The upper part of the figure shows the representation of the reaction matrix $\hat{M}$ by the Born terms of the potential $v_{eff} = U + \Delta U$, where ΔU describes the exchange of the pseudoparticles. [In the self-consistent approximation, the density matrix is expressed in terms of the $f(\vec{q},s)$.] The second part of the figure indicates, in a schematic fashion, the fact that the exchange of the pseudoparticles describes the role of correlations in the calculation of the reaction matrix $\hat{M}$.

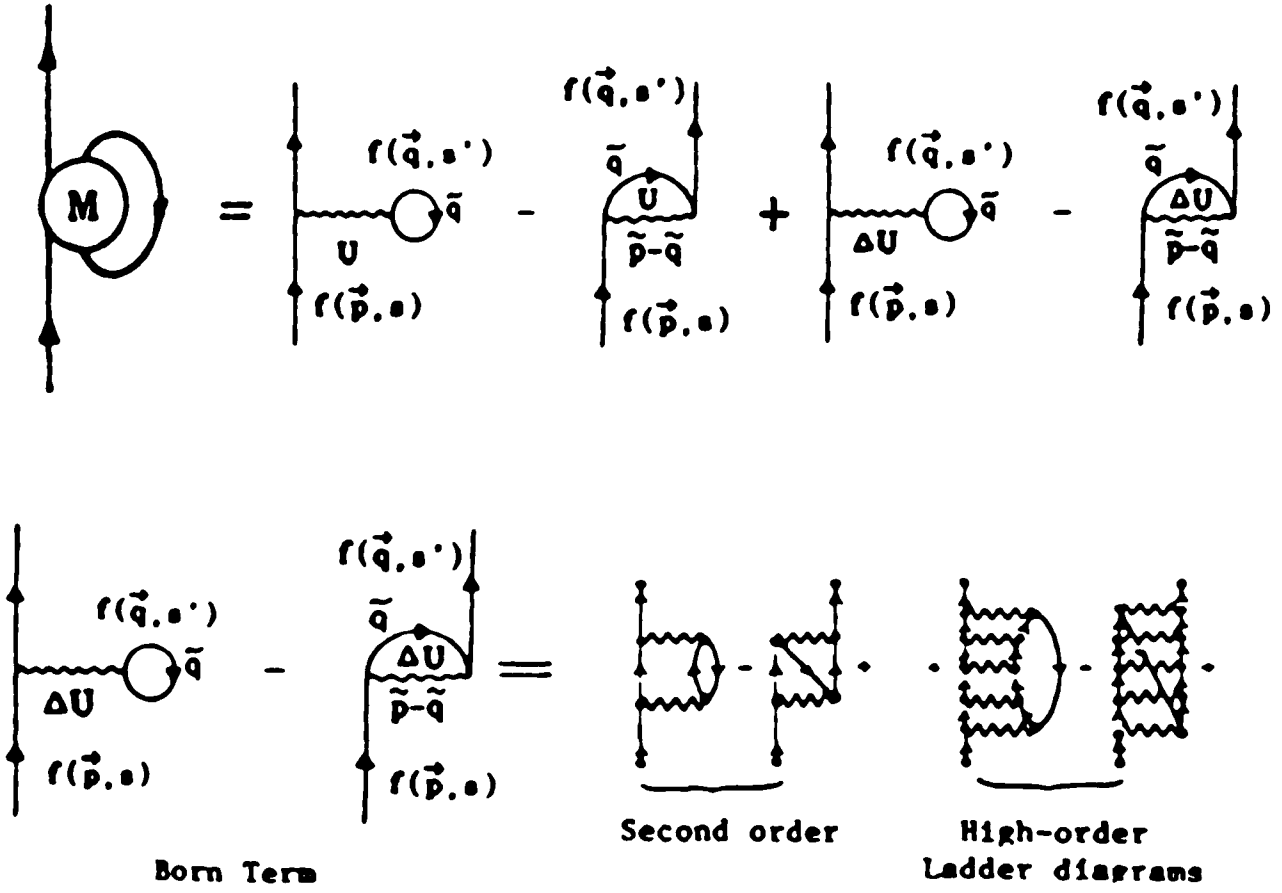
M
=
f(q⃗,s')
q̃
U
f(p⃗,s)
-
f(q⃗,s')
q̃
U
p̃-q̃
f(p⃗,s)
+
f(q⃗,s')
q̃
ΔU
f(p⃗,s)
-
f(q⃗,s')
q̃
ΔU
p̃-q̃
f(p⃗,s)
f(q⃗,s')
q̃
ΔU
f(p⃗,s)
-
f(q⃗,s')
q̃
ΔU
p̃-q̃
f(p⃗,s)
=
Born Term
Second order
High-order
Ladder diagrams

Fig. 1

Fig. 2:

Nuclear matter saturation curves of the relativistic quasiparticle method using the (density-dependent) parametrization given in Eq.(1.1) of Ref. 4. Curve a denotes the self-consistent result, while curve a' corresponds to a calculation in which the density matrix is expressed in terms of the spinors $u(\vec{p},s)$, instead of the (self-consistent) spinors $f(\vec{p},s)$.

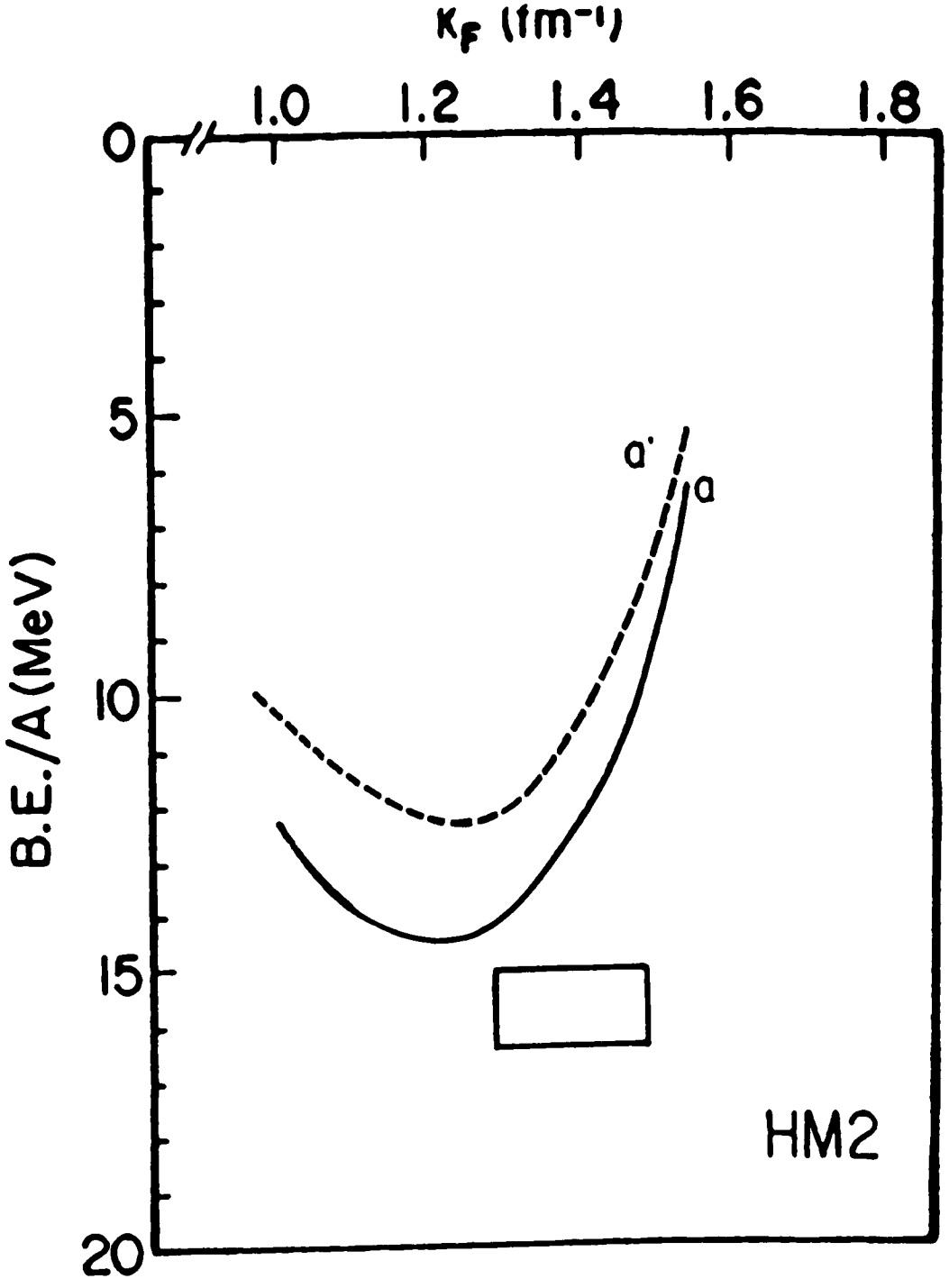

Fig. 2

Fig. 3:

Similar caption to that of Fig 2. Here, however, we neglect the density dependence of the pseudoparticle coupling constants and use the interaction defined by Eq.(1.1) of Ref. 4 at $\rho = \rho_{NM}$.

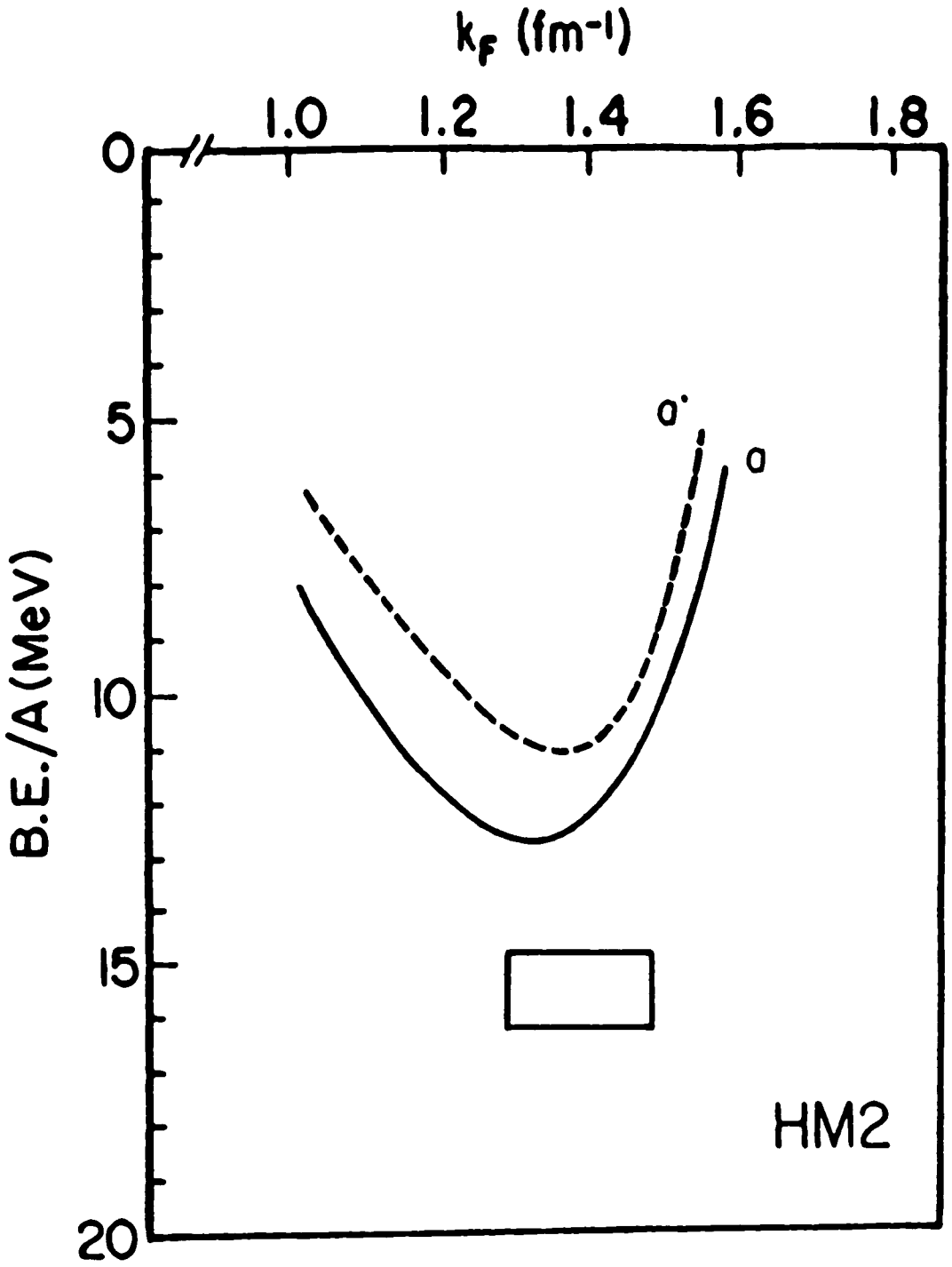

Fig. 3

Fig. 4:

a) The figure shows the amplitude for a nucleus of A nucleons to decay (virtually) into an off-mass-shell nucleon and an on-mass-shell residual system of (A-1) nucleons. The product of the vertex (open circle) and the propagator of the nucleon (of momentum k) defines a wave function (Ref. 8). The figure shows the equation which determines the wave function in terms of the self-energy, Σ.

b) Here we approximate the self-energy in terms of a reaction matrix, M, and a form factor of the (A-1)-body system.

c) The reaction matrix, $\hat{M}$, is replaced by the Born terms of our effective interaction. (A closed set of nonlinear equations is obtained by using the same vertex functions for the A-body and (A-1)-body systems.)

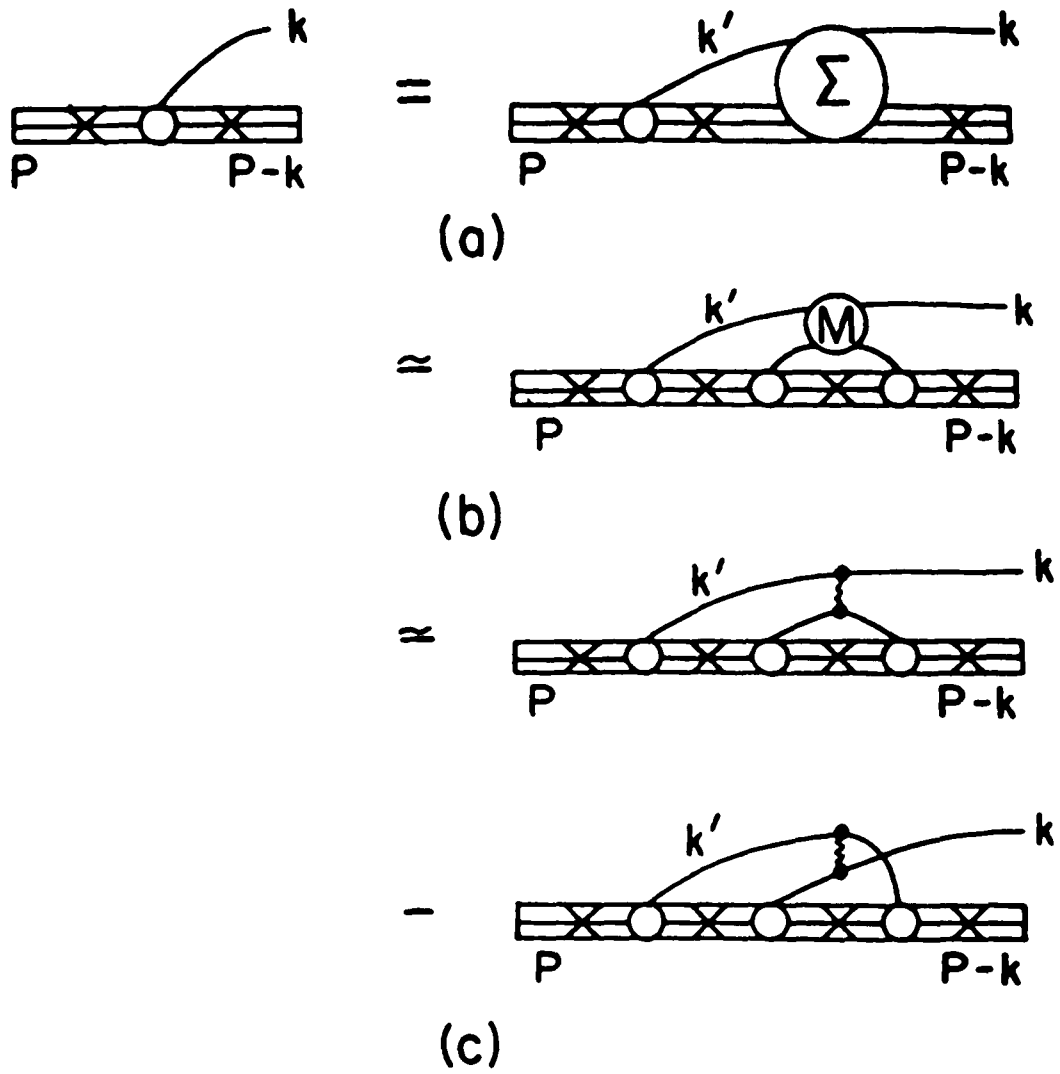

Fig. 4

Fig. 5:

Coordinate-space wave functions obtained for ^{16}O in a Dirac-Hartree-Fock calculation using the effective interaction based upon the interaction HM2.

a) The upper components, $R_U^{lj}(r)$, of the relativistic wave functions of ^{16}O obtained in this work. [See Eq. (3.2.1).]

b) Lower components of the wave functions of ^{16}O.

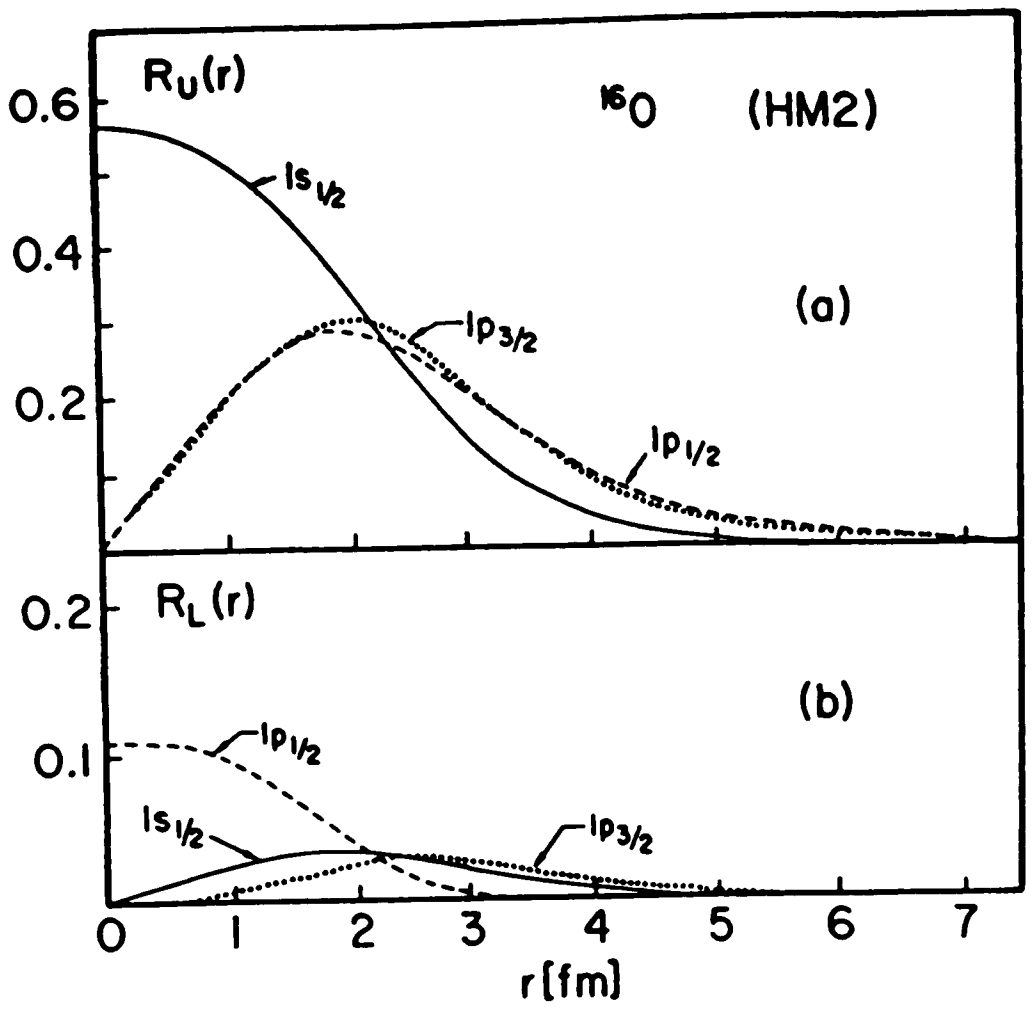
$R_U(r)$
^{16}O (HM2)
$1s_{1/2}$
$1p_{3/2}$
$1p_{1/2}$
(a)
0.6
0.4
0.2
$R_L(r)$
(b)
0.2
0.1
$1p_{1/2}$
$1s_{1/2}$
$1p_{3/2}$
0
1
2
3
4
5
6
7
r[fm]

Fig. 5

Fig. 6:

Same caption as Fig. 5, except that the nucleus studied is ^{40}Ca.

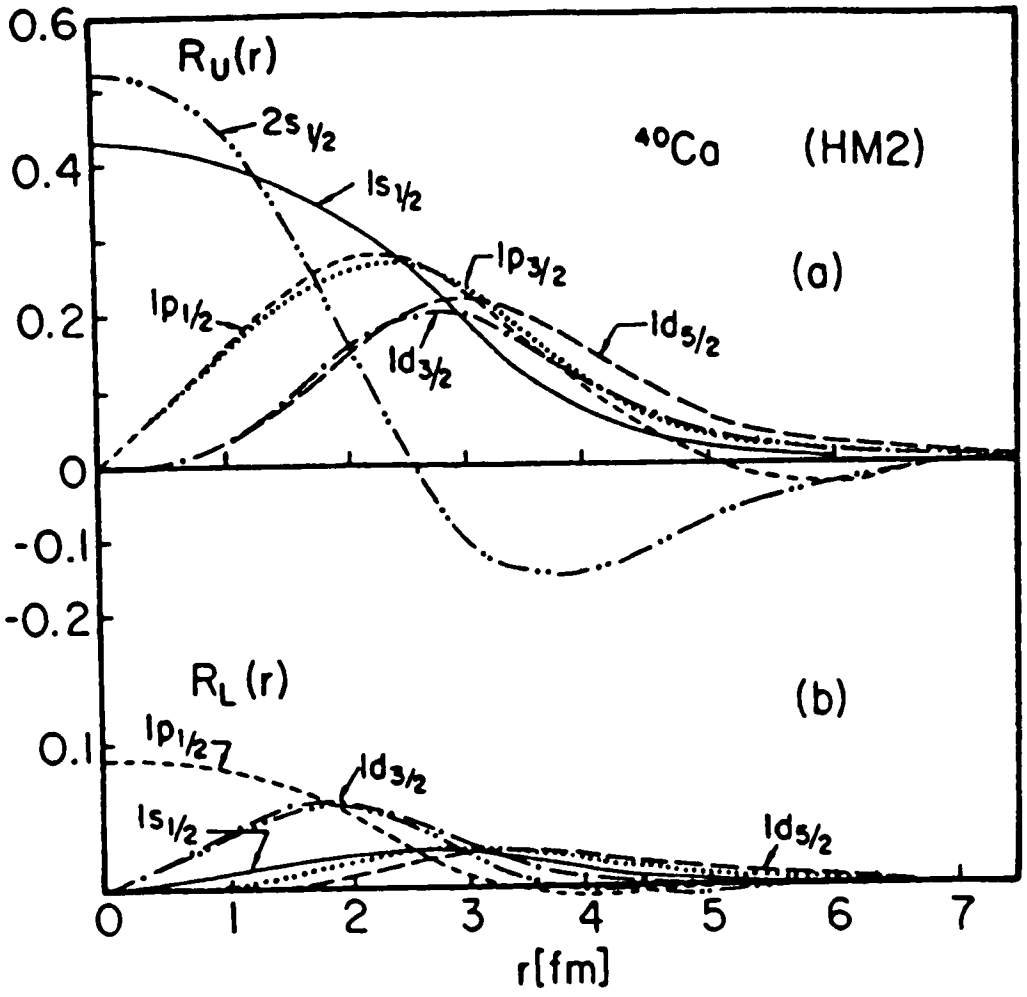
0.6
0.4
0.2
0
-0.1
-0.2
0.1
$R_U(r)$
$2s_{1/2}$
$1s_{1/2}$
^{40}Ca
(HM2)
(a)
$1p_{3/2}$
$1p_{1/2}$
$1d_{5/2}$
$1d_{3/2}$
$R_L(r)$
(b)
$1p_{1/2}$
$1d_{3/2}$
$1s_{1/2}$
$1d_{5/2}$
0
1
2
3
4
5
6
7
r[fm]

Fig. 6

Fig. 7:

Momentum-space wave functions obtained for ^{16}O in a Dirac-Hartree-Fock calculation using the effective interaction based upon the interaction HM2.

a) The upper component, $R_U^{lj}(k)$, of the relativistic wave functions obtained in this work.[See Eq. (3.2.1).]

b) Lower components of the wave functions of ^{16}O.

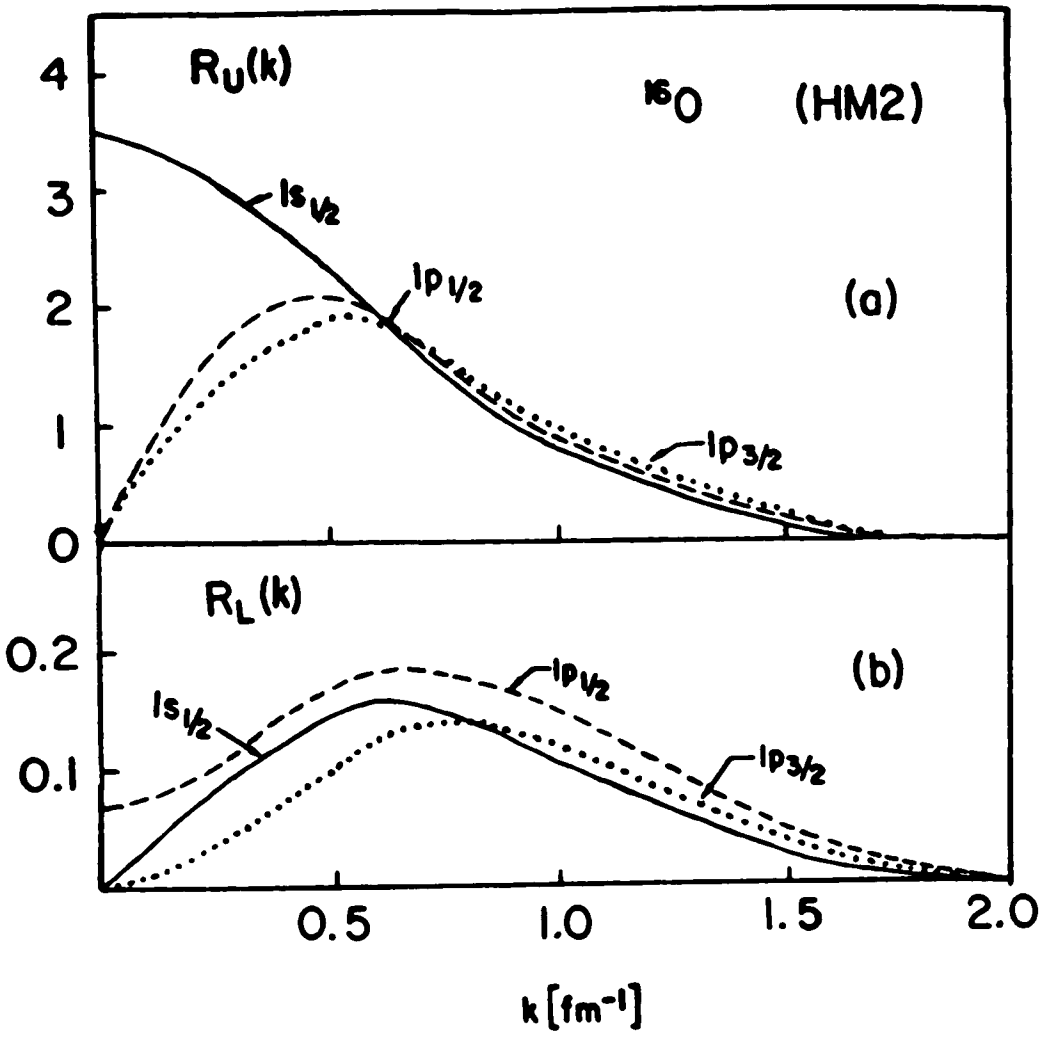
$R_U(k)$
^{16}O (HM2)
$1s_{1/2}$
$1p_{1/2}$
(a)
$1p_{3/2}$
$R_L(k)$
(b)
$1p_{1/2}$
$1s_{1/2}$
$1p_{3/2}$
4
3
2
1
0
0.2
0.1
0.5
1.0
1.5
2.0
k [fm^{-1}]

Fig. 7

Fig. 8:

Same caption as Fig. 7, except that the nucleus studied is ^{40}Ca.

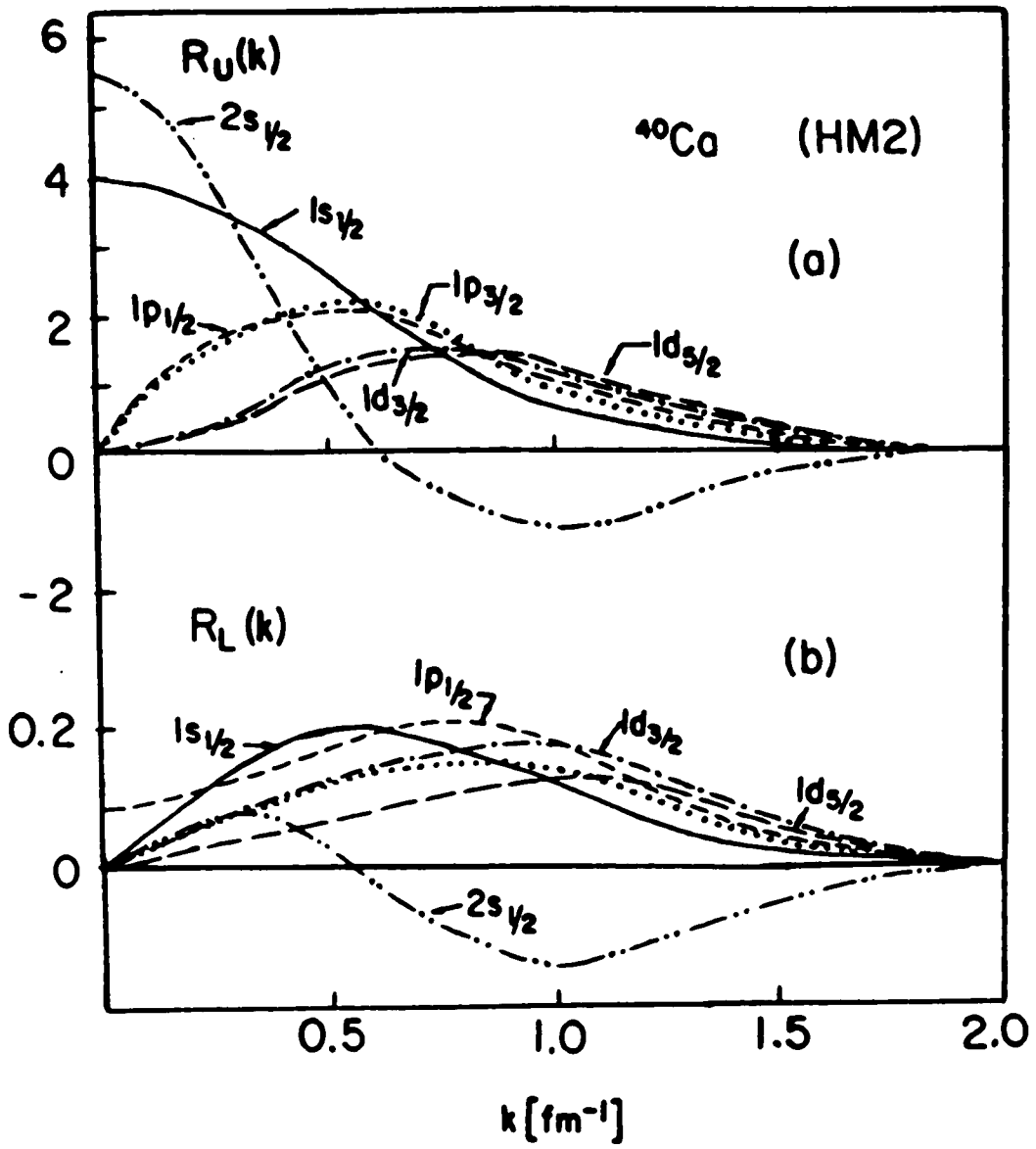
6
4
2
0
-2
0.2
0
$R_U(k)$
$2s_{1/2}$
^{40}Ca (HM2)
$1s_{1/2}$
(a)
$1p_{3/2}$
$1p_{1/2}$
$1d_{5/2}$
$1d_{3/2}$
$R_L(k)$
(b)
$1p_{1/2}$
$1d_{3/2}$
$1s_{1/2}$
$1d_{5/2}$
$2s_{1/2}$
0.5
1.0
1.5
2.0
k [fm^{-1}]

Fig. 8

Fig. 9:

A contour plot of the potential $A(k,k',\cos\theta)$ obtained for ^{40}Ca is shown for $\theta = 0$. [The effective interaction corresponding to the potential HM2 has been used.]

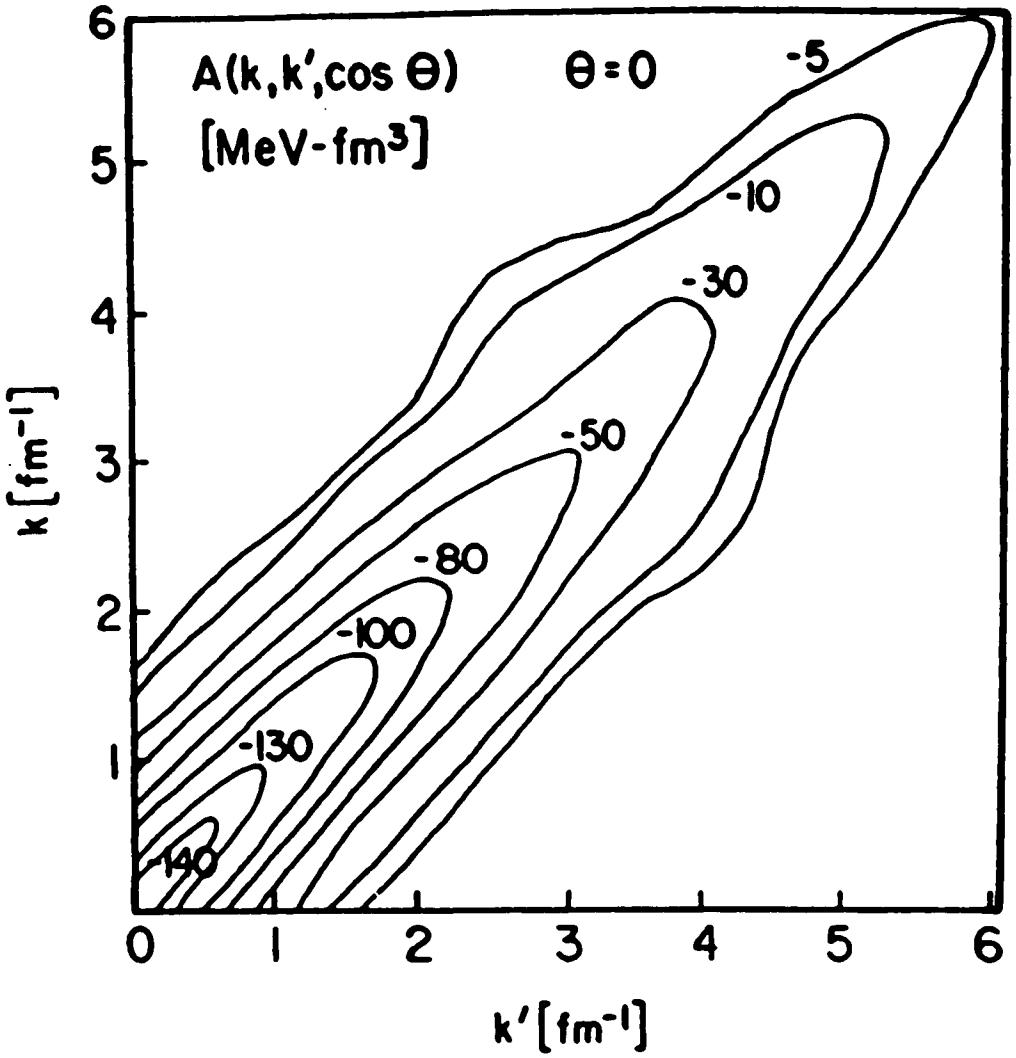

Fig. 9

Fig. 10:

The potential $B(k,k',\cos\theta)$ is shown for $\theta = 0$. [See caption of Fig. 9.]

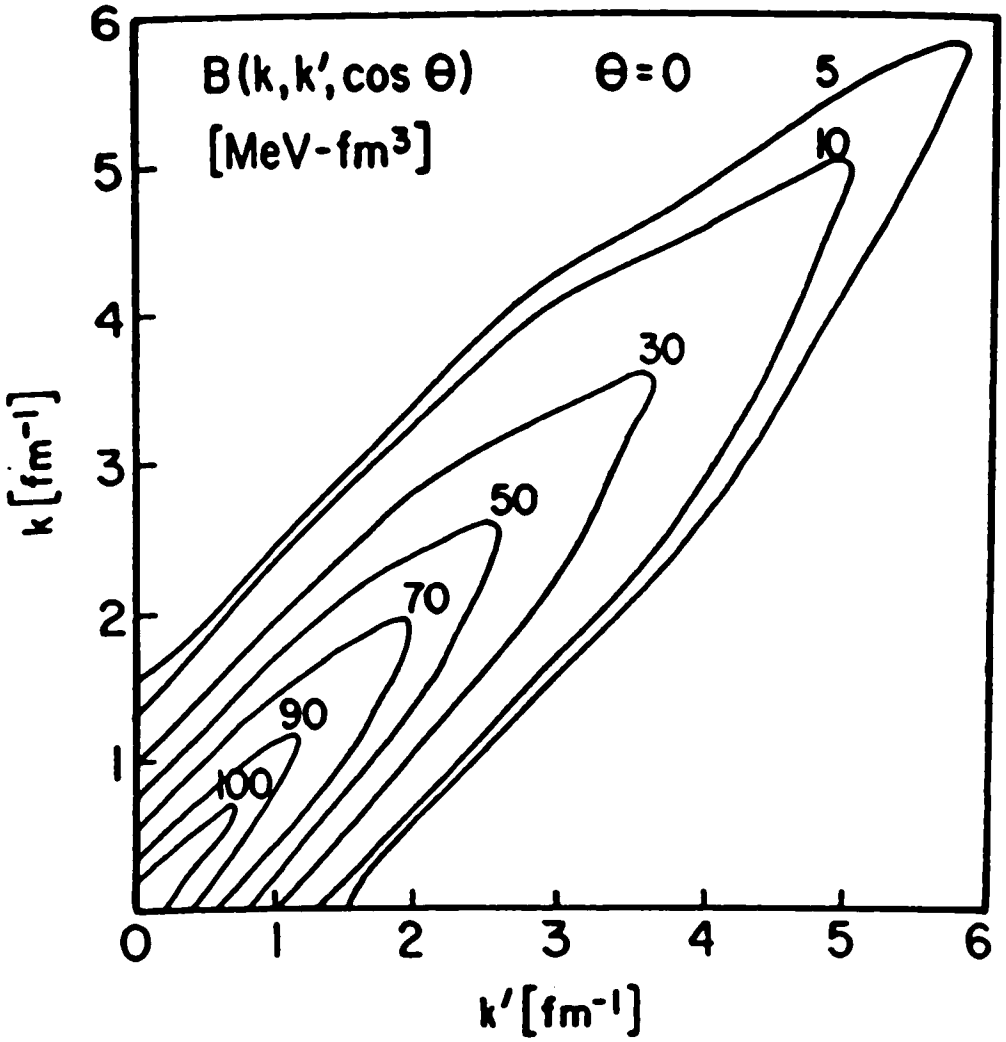

Fig. 10

Fig. 11:

The potential $C(k,k',\cos\theta)$ is shown for $\theta = 0$. [See caption of Fig. 9.]

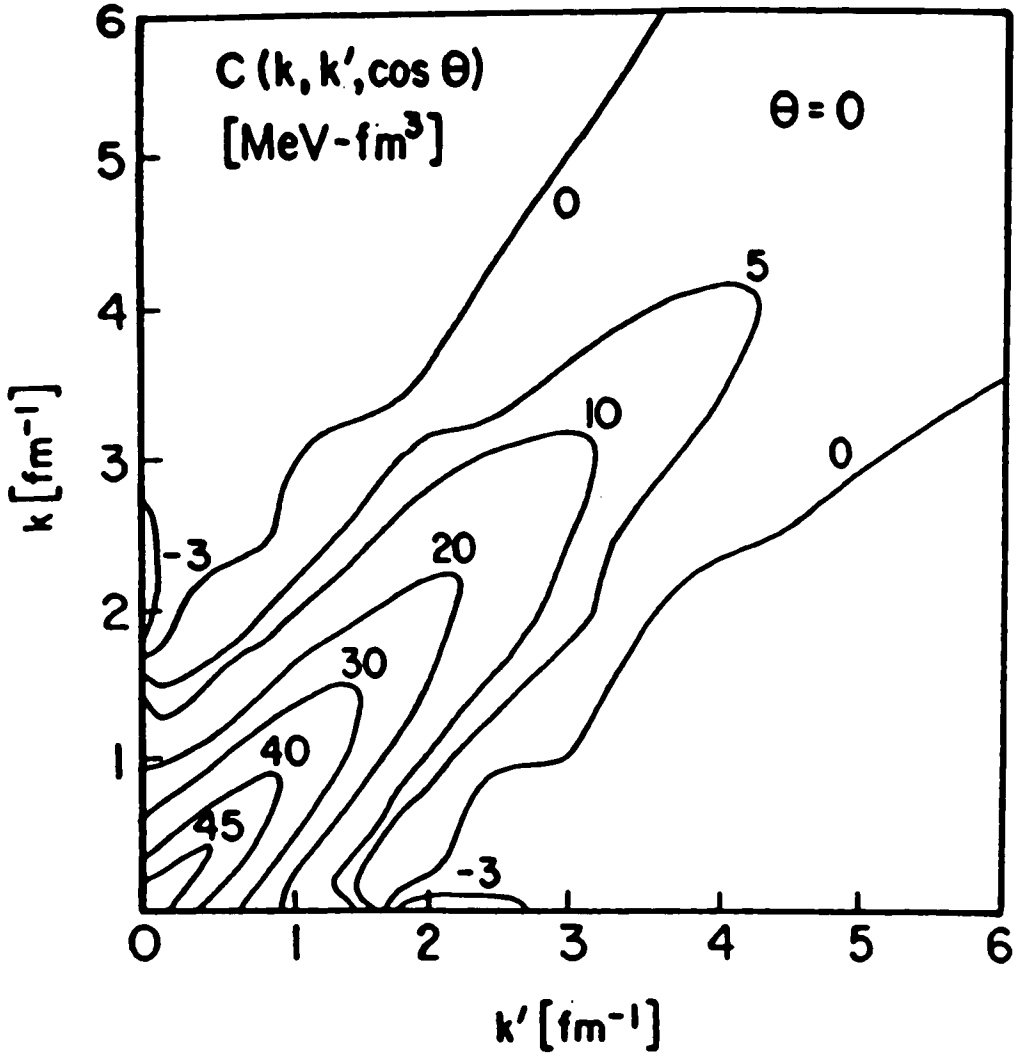

Fig. 11

Fig. 12:

The potential $E(k,k',\cos\theta)$ is shown for $\theta = 0$. [See caption of Fig. 9.]

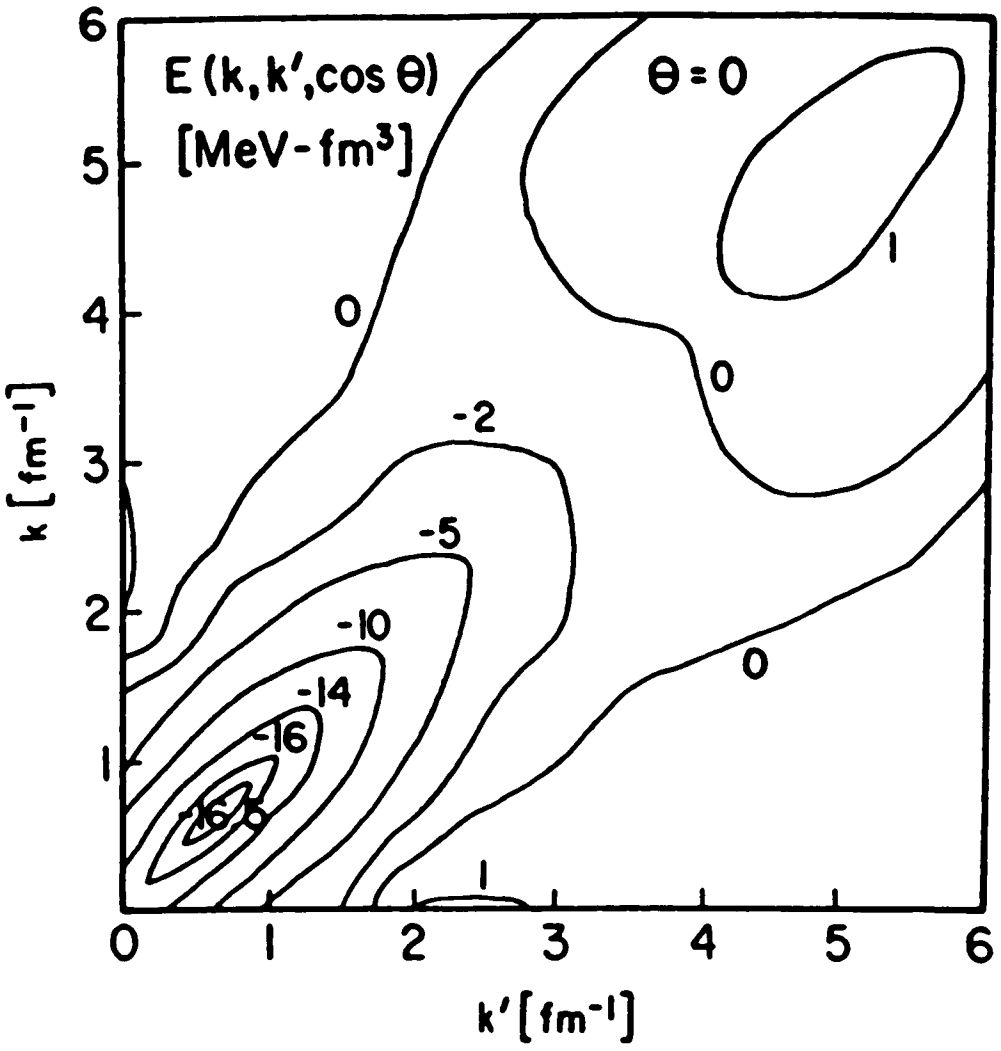

Fig. 12

Fig. 13:

The potential $H(k,k',\cos\theta)$ is shown for $\theta = 0$. [See caption of Fig. 9.]

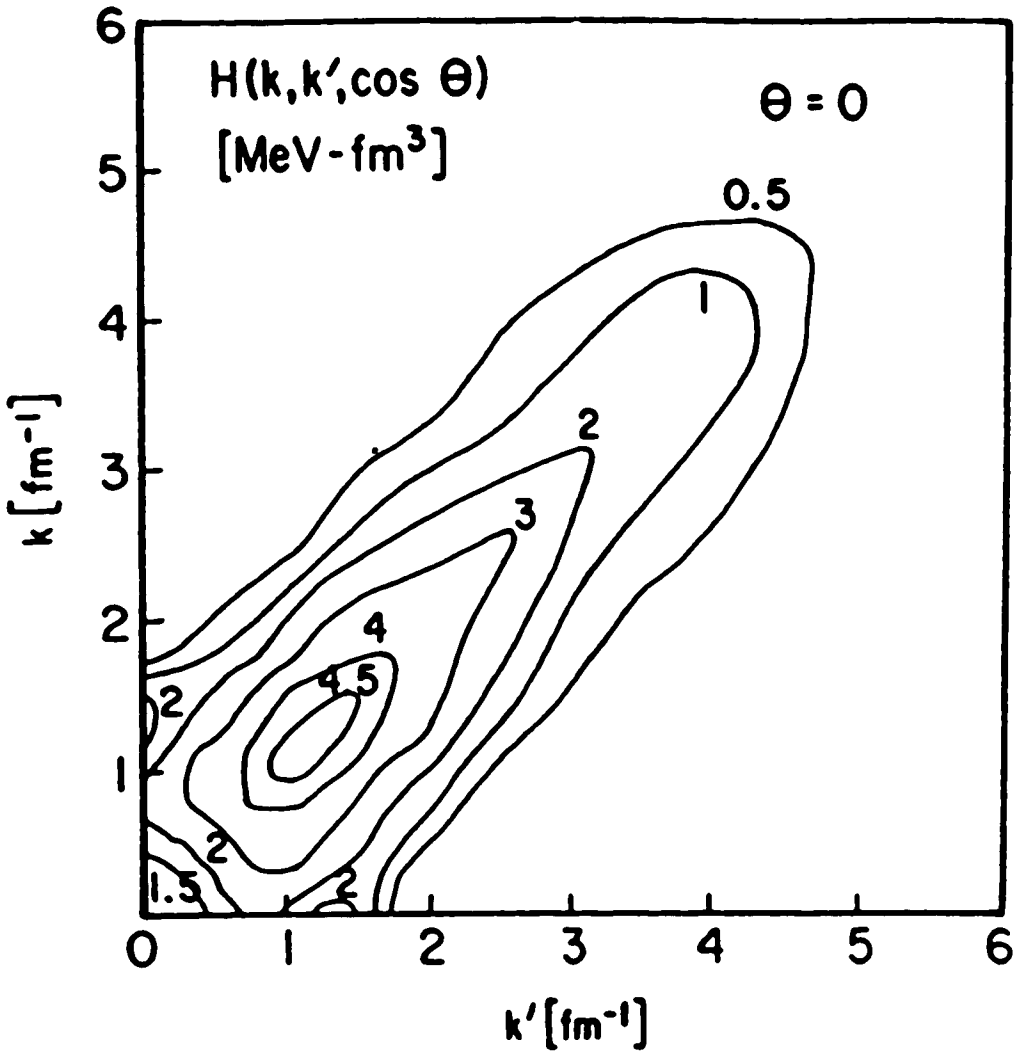

Fig. 13

Fig. 14:

The experimental charge distribution of ^{16}O is shown (solid line and cross-hatched region). The dashed line is the result of Horowitz and Serot (Ref. 10), while the dash-dot line is our result for the effective interaction based upon OBEP HM2. The dash-dot line follows the experimental data to the degree that it cannot be distinguished in the figure from the solid line for $r > 1$ fm.

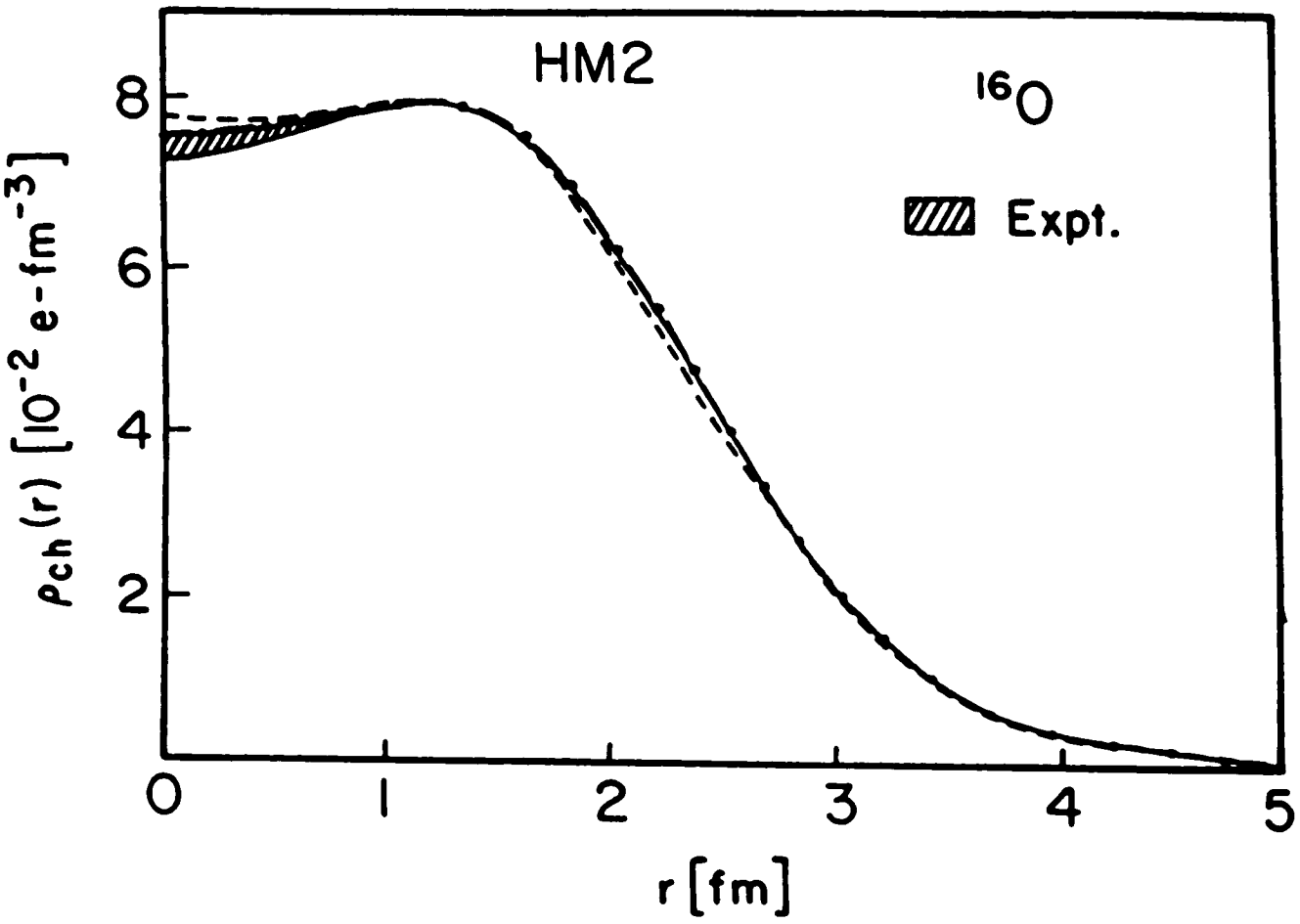

Fig. 14

Fig. 15:

The experimental charge distribution for ^{40}Ca is shown (solid line and cross-hatched area). The dashed line shows the early result of Horowitz and Serot (Ref. 10), who adjusted the parameters of their calculation to give the correct charge radius of ^{40}Ca in a Dirac-Hartree approximation. The result of our calculation is shown as the dash-dot line for the effective interaction based upon OBEP HM2.

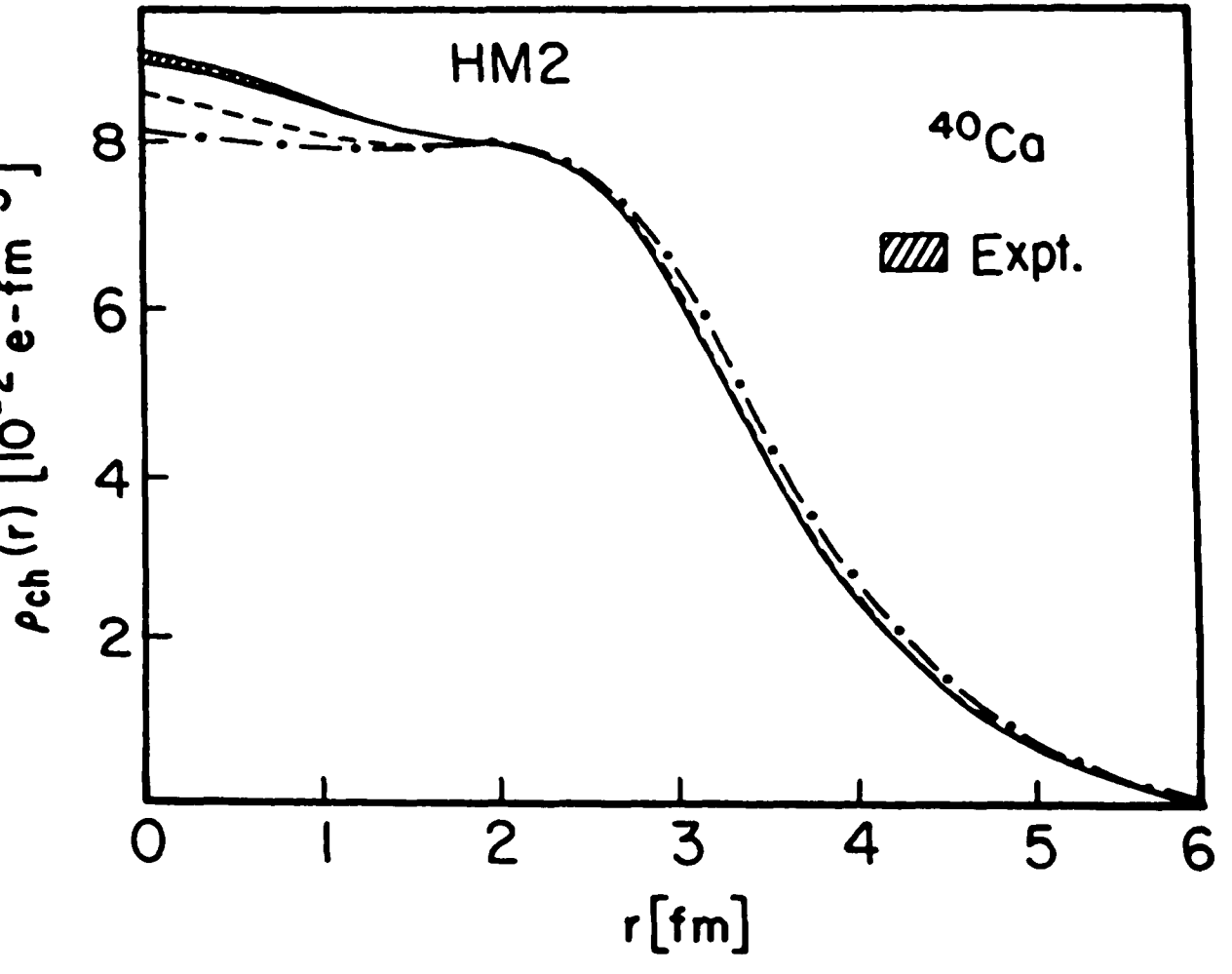

Fig. 15

Fig. 16:

The experimental charge distribution of ^{16}O is shown (solid line and cross-hatched region). The dash-dot line is our result for the effective interaction based upon OBEP HEA.

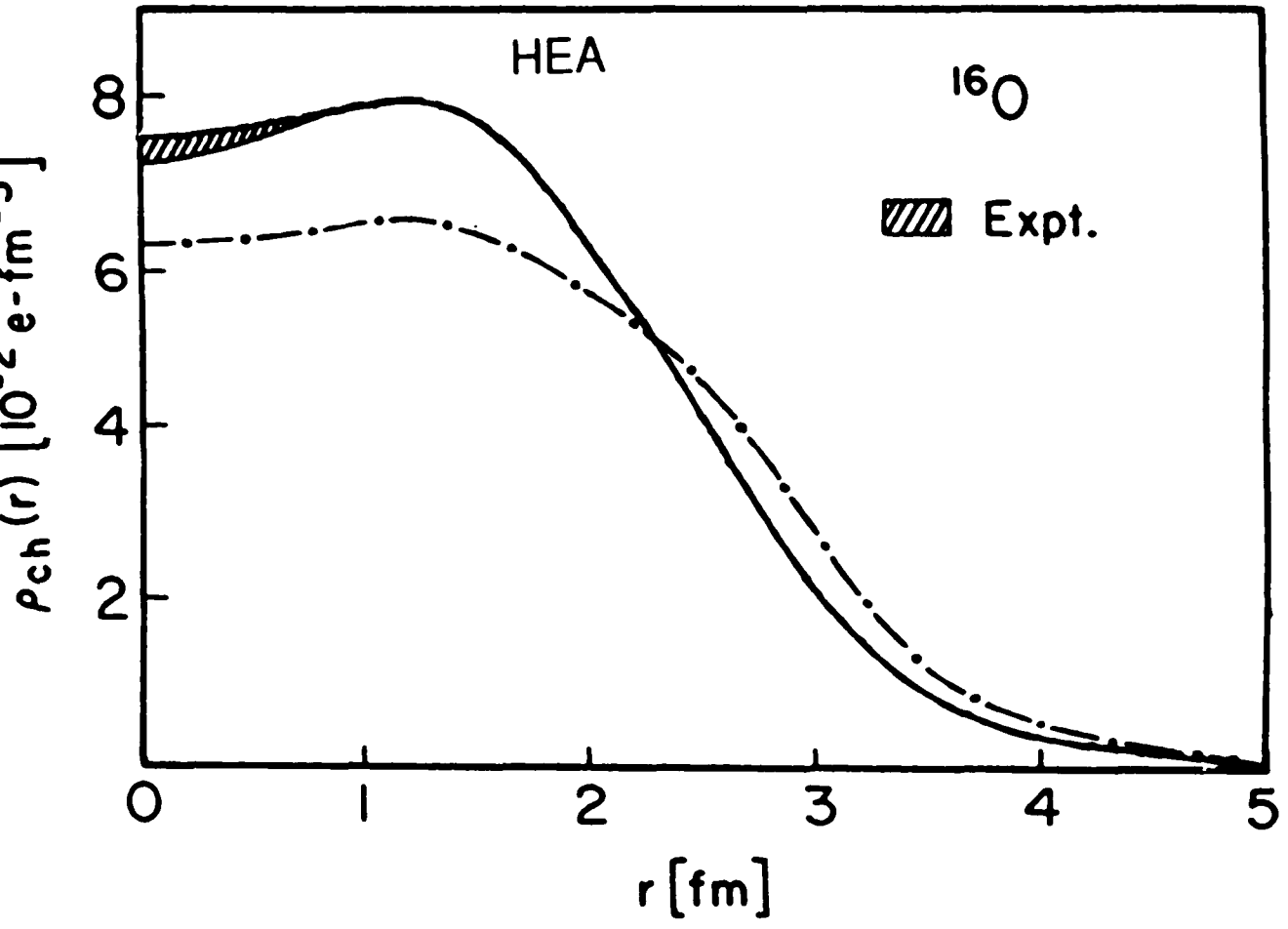

Fig. 16

Fig. 17:

The experimental charge distribution for ^{40}Ca is shown (solid line and cross-hatched area). The result of our calculation is shown as the dash-dot line for the effective interaction based upon OBEP HEA.

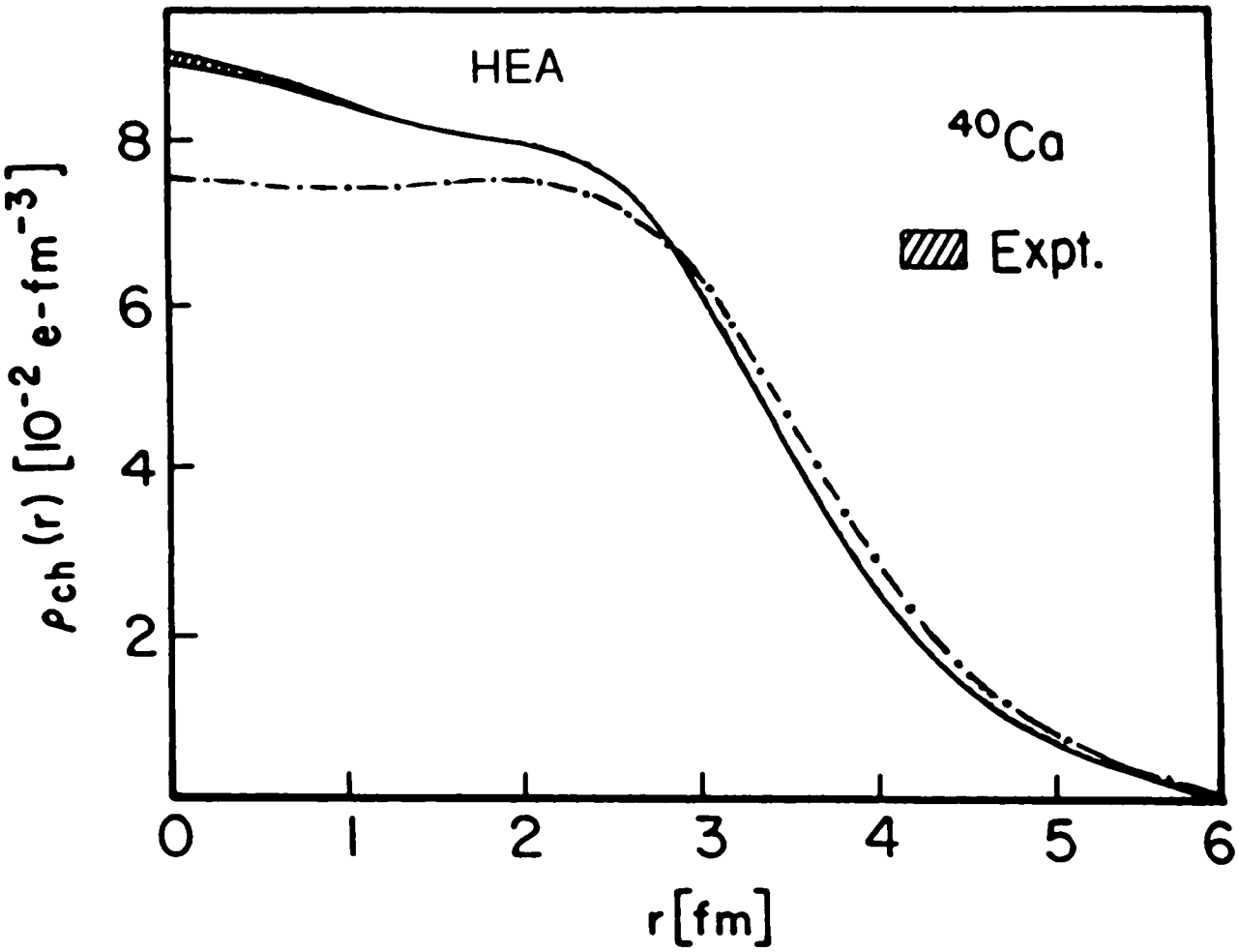

Fig. 17

References

1. For reviews of the boson-exchange model see, K. Erkelenz, Phys. Rep. 13, 191 (1974) and K. Holinde, Phys. Rep. 68, 122 (1981).

2. H. Muther, R. Machleidt and R. Brockman, Phys. Lett. 202B, 483 (1988). See also, Y.J. Lee, C. Nuppenau and A.D. MacKellar, University of Kentucky, preprint (1989). R. Brockman and R. Machleidt, Phys. Lett. 149B, 283 (1984).

3. H.S. Ai, L.S. Celenza, A. Harindranath and C.M. Shakin, Phys. Rev. C35, 2299 (1987).

4. Hsiao-bai Ai, L.S. Celenza, Shun-fu Gao and C.M. Shakin ,Phys. Rev. C39, 236 (1989).

5. L.S. Celenza and C.M. Shakin, Relativistic Nuclear Physics: Theories of Structure and Scattering (World Scientific, Singapore, 1986).

6. L.S. Celenza, A. Harindranath, A. Rosenthal and C.M. Shakin, Phys. Rev. C31, 946 (1985).

7. K. Holinde, K. Erkelenz and R. Alzetta, Nucl. Phys. A198, 598 (1972).

8. K. Holinde and R. Machleidt, Nucl. Phys. A256, 479 (1976).

9. C.M. Shakin and M.S. Weiss. Phys. Rev. C15, 1911 (1977).

10. C.J. Horowitz and B.D. Serot, Nucl. Phys. A368, 503 (1981).

11. For a review and discussion of related work, see R. Machleidt, The Meson Theory of Nuclear Forces and Nuclear Structure, in Advances in Nuclear Physics, Vol. 19, Edited by J.W. Negele and E. Vogt (Plenum Press, New York, in press).

12. L.S. Celenza and C.M. Shakin, Brooklyn College Report: B.C.I.N.T 97/071/79 (1979).

13. A. Harindranath, Ph. D. Dissertation: Studies in Relativistic Nuclear Physics (City University of New York, 1985).

14. J.D. Bjorken and S.D. Drell, Relativistic Quantum Mechanics (McGraw Hill, New York, 1964).